Article

Not peer-reviewed version

Evolutionary History and Distribution Analysis of Rhamnosyltransferases in the Fungal Kingdom

Joaquín Omar Chávez-Santiago , Luz A. López-Ramírez , Luis A. Pérez-García , Iván Martínez-Duncker , Bernardo Franco , Israel Enrique Padilla-Guerrero , Vianey Olmedo-Monfil , J. Felix Gutiérrez Corona , Gustavo A. Niño-Vega , Jorge H. Ramírez-Prado , Héctor M. Mora-Montes *

Posted Date: 28 May 2025

doi: 10.20944/preprints202505.2096.v1

Keywords: rhamnosyltransferases; evolutionary history: fungal kingdom; protein glycosylation; Hidden Markov models

 doi:10.20944/preprints202505.2096.v1

Article

Evolutionary History and Distribution Analysis of Rhamnosyltransferases in the Fungal Kingdom

Joaquín O. Chávez-Santiago [1], Luz A. López-Ramírez [1], Luis A. Pérez-García [2], Iván Martínez-Duncker [3], Bernardo Franco [1], Israel E. Padilla-Guerrero [1], Vianey Olmedo-Monfil [1], J Félix Gutiérrez-Corona [1], Gustavo A. Niño-Vega [1], Jorge H. Ramírez-Prado [4,*,†] and Héctor M. Mora-Montes [1,*,†]

[1] Universidad de Guanajuato

[2] Facultad de Estudios Profesionales Zona Huasteca, Universidad Autónoma de San Luis Potosí, Romualdo del Campo 501, Fracc. Rafael Curiel, 79060, Ciudad Valles, S.L.P., Mexico

[3] Laboratorio de Glicobiología Humana y Diagnóstico Molecular, Centro de Investigación en Dinámica Celular, Instituto de Investigación en Ciencias Básicas y Aplicadas, Universidad Autónoma del Estado de Morelos, Cuernavaca Mor. 62209, México

[4] Unidad de Biotecnología, Centro de Investigación Científica de Yucatán, A. C., Calle 43 No. 130, Col. Chuburná de Hidalgo, Mérida, Yucatán 97205, Mexico

* Correspondence: jhramirez@cicy.mx (J.H.R.-P.); hmora@ugto.mx (H.M.M.-M.)

† Both authors equally contributed to this work.

Abstract: Rhamnose is a natural sugar found in glycoproteins and structural polysaccharides of plants, fungi, and bacteria. Its incorporation into glycoconjugates is mediated by rhamnosyltransferases (RHTs), key enzymes for biomolecular stability and function. While rhamnose biosynthesis has been studied in certain fungal genera, the evolutionary history and distribution of RHTs across the fungal kingdom remain largely unknown. In this study, 351 fungal species were found to encode putative RHTs. Phylogenetic and structural analyses revealed conserved patterns and similarities with previously characterized RHTs. Molecular docking predicted a high affinity of these proteins for UDP-L-rhamnose, and in silico mutagenesis identified key residues potentially involved in substrate binding. Carbohydrate profiling confirmed the presence of rhamnose in the cell walls of multiple fungi, including *Aspergillus*, *Madurella*, *Metarhizium*, and *Trichoderma* species. Enzymatic assays further supported rhamnose transfer activity. These findings provide the first comprehensive in silico characterization of fungal RHTs, uncovering conserved sequence motifs despite overall diversity, which may be linked to functional adaptation in different fungal lineages.

Keywords: rhamnosyltransferases; evolutionary history: fungal kingdom; protein glycosylation; Hidden Markov models

1. Introduction

The kingdom Fungi originated approximately 500 to 1000 million years ago and is one of the most extensive eukaryotic kingdoms, with approximately 1.5 to 5 million species [1,2]. This kingdom is composed of highly diverse organisms that exhibit a wide variety of life cycles, morphologies, and metabolisms, inhabiting almost all ecosystems and interacting in various ways with species in their environment by developing mutualistic, parasitic, and commensal relationships [2].

It is composed of eukaryotic, heterotrophic organisms characterized by cellular structures that range from simple unicellular organisms to more complex filaments capable of forming macroscopic organisms [3,4]. Fungi have abilities that allow them to thrive in different environments, colonize plant and animal cells, and contribute to the nutrient cycle in both terrestrial and aquatic environments [4].

 doi:10.20944/preprints202505.2096.v1

Fungi possess a cell wall responsible for safeguarding cellular integrity to withstand the various conditions to which these organisms are subjected. Its characteristics can vary depending on the species, but it is generally enriched with polysaccharides that can vary in composition and structural organization [5,6]. Among the most important cell wall structural polysaccharides are chitin, β-1,3-glucans, β-1,6-glucans, and glycoproteins [5,7,8].

Among these polysaccharides, glycoproteins are assembled by glycosyltransferases (GTs), which are enzymes found in animals, protists, plants, bacteria, and fungi. These play key roles in biological processes by transferring sugars to other receptor molecules, such as carbohydrates and proteins, as well as contributing to the formation of the cell wall and the glycosylation of metabolites [9,10].

UDP-glycosyltransferases (UGTs) are among the most studied GTs; these belong to the GT1 family and possess GT-B folds [11]. They can transfer UDP-sugars, such as UDP-glucose, UDP-galactose, UDP-xylose, and UDP-rhamnose to their receptors, which include polysaccharides, proteins, lipids, and secondary metabolites [12–14]. Among these sugars, UDP-rhamnose has been studied to a lesser extent, despite being relevant for the cellular viability of some fungi. This is the case for genera such as *Sporothrix* and *Scedosporium*, where rhamnose-based glycoconjugates are structural cell wall components [13–15]. In *Paracoccidioides brasiliensis*, rhamnose is part of the glucuronoxylomannan-like glycans, a heteropolysaccharide essential for its virulence [16]. UGTs responsible for transferring UDP-rhamnose are known as rhamnosyltransferases (RHTs), and biochemical analyses revealed the existence of two UDP-rhamnose-dependent rhamnosyltransferases in *S. schenckii* [8].

Although UGT protein sequences from different species do not exhibit high identity, UGTs structures possess GT-B folds that show high conservation [9]. The GT-B fold comprises two independent Rossman-type β/α/β domains, consisting of an N-terminal domain and a C-terminal domain, which are positioned face-to-face and connected by an interdomain cleft. These domains are responsible for recognizing and binding UDP-sugar donors with their respective acceptors [10,17].

In the kingdom Plantae, the presence of RHTs has been confirmed, for example in *Arabidopsis thaliana*, whose cell wall contains pectin, specifically rhamnogalacturonan I (RG-I). The enzyme RRT1, belonging to the GT106 glycosyltransferase family, participates in RG-I synthesis by transferring rhamnose from UDP-β-L-rhamnose, playing a key role in the formation of the plant cell wall [18]. In the case of the kingdom of Fungi, the available information is insufficient to detail the rhamnosyltransferases' evolutionary history. For this reason, in this study, we conducted a bioinformatic search for potential genes encoding enzymes involved in the rhamnosylation of other molecules in the kingdom Fungi. To identify these hypothetical genes, we used hidden Markov model (HMM) profiles, identified the main motifs found in these sequences, and compared them to analyze their distribution across different taxonomic groups within the kingdom Fungi. Additionally, we performed molecular docking assays to predict the binding affinity between the potential RHTs and UDP-rhamnose and provide experimental evidence of the presence of rhamnosyltransferases in some of the identified species.

2. Materials and Methods

2.1. Hardware and Software Environment Used

All bioinformatic analyses were conducted on an HP ENVY x360 with AMD Ryzen 3 2300u 2.00 GHz, 8 GB RAM, 256 GB SSD, an external ADATA HV620S 1TB hard drive, and Windows Subsystem for Linux (WSL), a compatibility layer developed by Microsoft to run Linux binaries (in ELF format) natively on Windows 10. The analyses were performed on publicly accessible servers: NCBI databases [19], PFAM database [20], and AlphaFold2 hosted on Google Colab [21].

 doi:10.20944/preprints202505.2096.v1

2.2. Downloading the NCBI Database

The non-redundant (NR) BLAST database was downloaded on October 9, 2023, directly from the NCBI platform. The command used for downloading was:

sudo wget -p /mnt/adata https://ftp.ncbi.nlm.nih.gov/blast/db/nr.00.tar.gz

2.3. Construction of Hidden Markov Models of Rhamnosyltransferases and HMMER Searches

Protein sequences of rhamnosyltransferases from *Sporothrix schenckii* (Genebank accession code given in brackets) SPSK_05538 (XP_016583713.1) and SPSK_01110 (XP_016584143.1) were downloaded directly from the NCBI database [8]. Additionally, a tblastn search was conducted within the genomes of *S. brasiliensis* (GCF_000820605.1), *S. globosa* (GCA_001630435.1), *S. dimorphospora* (GCA_021397985.1), *S. pallida* (GCA_021396235.1), *S. luriei* (GCA_021398005.1), *S. humícola* (GCA_021396245.1), *S. mexicana* (GCA_021396375.1), *S. phasma* (GCA_016097075.2), *S. variecibatus* (GCA_016097105.2), *S. inflata* (GCA_021396225.1), *S. euskadiensis* (GCA_019925375.1), *S. pseudoabietina* (GCA_019925295.1), *S. curviconia* (GCA_016097085.2), *S. brunneoviolacea* (GCA_021396205.1), *S.* cf. *nigrograna* (GCA_019925305.1), *S. protearum* (GCA_016097115.2), and *Niveomyces insectorum* (GCA_001636815.1).

Following this, a "blastdbcmd" command was used within WSL to retrieve nucleotide sequences from the analyzed species based on accession numbers and ranges obtained from tblastn searches [22].

blastdbcmd -db database_name -entry sequence_accession_number -range tblastn_range_obtained -out new_filename -outfmt output_format

Once amino acid sequences were obtained, multiple sequence alignment (MSA) was performed using the MAFFT algorithm (v. 7) [23].

For the Rht1 protein (SPSK_05538, XP_016583713.1), eight sequences were discarded due to high divergence. The remaining eight sequences (*S. schenckii*, *S. brasiliensis*, *S. globosa*, *S. mexicana*, *S. humícola*, *S. dimorphospora*, *S. inflata*, and *S. pallida*) were realigned using the MAFFT algorithm, and the resulting alignment was saved in STOCKHOLM format (SPSK_05538_MAFFT.sto). Similarly, for the Rht2 protein (SPSK_01110, XP_016584143.1), eight highly divergent sequences were discarded, and the remaining eight sequences (*S. schenckii*, *S. brasiliensis*, *S. globosa*, *S. mexicana*, *S. humícola*, *S. dimorphospora*, *S. inflata*, and *S. variecibatus*) were realigned and saved in STOCKHOLM format (SPSK_01110_MAFFT.sto).

In addition to the RHTs sequences, orthologous sequences of the *RmlD* gene (which is involved in rhamnose biosynthesis), SPSK_06451 (XP_016591762.1), from genus *Sporothrix*, were also retrieved. A total of 13 sequences were obtained from the following species: *S. schenckii* (XP_016591762.1), *S. brasiliensis* (XP_040615952.1), *S. globosa* (LVYW01000006.1), *S. luriei* (WNLO01000074.1), *S. dimorphospora* (WOUA01000046.1), *S. inflata* (WNYF01000047.1), *S. pallida* (WNYG01000035.1), *S. humicola* (WNYE01000047.1), *S. mexicana* (WNYC01000019.1), *S. euskadiensis* (JADHKQ010000009.1), *S. pseudoabietina* (JADHKS010000001.1), *S. protearum* (JADMNH010000019.1), and *N. insectorum* (OAA58952.1). The 13 sequences were aligned using the MAFFT algorithm and saved in STOCKHOLM format (SPSK_06451_MAFFT.sto).

Subsequently, HMM profiles were generated from the MSAs of Rht1, Rht2, and RmlD using the "hmmbuild" command from locally installed HMMER (v. 3.3.2) on WSL [24].

hmmbuild SPSK_05538.hmm SPSK_05538_MAFFT.sto
hmmbuild SPSK_01110.hmm SPSK_01110_MAFFT.sto
hmmbuild SPSK_06451.hmm SPSK_06451_MAFFT.sto

Later, searches were conducted using the HMM profiles of Rht1, Rht2, and RmlD, using the "hmmsearch" command from HMMER, against the protein database of the kingdom Fungi obtained from NCBI (fungi_prot_db.fa).

Hmmsearch SPSK_05538.hmm fungi_prot_db.fa > SPSK_05538_MAFFT.hmmsearch
Hmmsearch SPSK_01110.hmm fungi_prot_db.fa > SPSK_01110_MAFFT.hmmsearch
Hmmsearch SPSK_06451.hmm fungi_prot_db.fa > SPSK_06451_MAFFT.hmmsearch

 doi:10.20944/preprints202505.2096.v1

Finally, to determine the possible domains present in the retrieved sequences, an E-value cutoff of $E<1x10^{-20}$ (1e-20) was established [25]. These sequences were saved in a multi-sequence FASTA file format.

2.4. Distribution of Potential RHTs in the Kingdom Fungi

The distribution analysis of motifs in the putative RHTs was performed using the MEME Suite [26]. Protein sequences obtained from the searches conducted with HMMER for Rht1 and Rht2 were employed. The "Classic mode" configuration was used with "Any number of repetitions" in the site distribution, and the goal was to identify exactly five motifs. Advanced options- maintained default conditions, adjusting only the motif size to search, with a minimum of "6" and a maximum of "20".

To infer phylogenetic relationships of putative RHTs proteins, sequence alignments were generated using MAFFT [23], and phylogenetic trees were constructed with PhyML 3.0 [27] using the parameters '-model BIC -Starting tress BioNJ -Fast likehood-based methods aLRT SH-like'.

2.5. Analysis of Three-Dimensional Structures of Putative RHTs

The sequences previously selected in the conserved motif analysis were used. Initially, a search was conducted in the Uniprot database to obtain the files containing a predicted three-dimensional model of the proteins in 'Protein Data Bank' (.PDB) format [28]. Sequences whose three-dimensional structure was not found in the Uniprot database were modeled from their amino acid sequence using Alphafold 2 [21]. These files were subsequently analyzed using the PyMOL software [29], which allows for visualization of the three-dimensional structures and alignment between multiple structures.

RHTs putative sequences were analyzed using the CB-Dock and PyRx [30,31], where interactions between ligands and proteins were analyzed. Additionally, Discovery Studio was also used for the 2D visualization of the protein–ligand docking complex structure [32].This approach enabled the prediction of binding affinities between the putative RHTs and UDP-L-rhamnose (CID: 192751), UDP-glucose (CID: 8629), GDP-mannose (CID: 135398627), and dolichol phosphate mannose (SID: 5646075); all obtained from PubChem [33] database in SDF file format.

Docking analyses were performed using PyRx software, where ligands were processed in Open Babel for energy minimization through charge addition and optimization with the universal force field [34]. The binding energy values of the docked ligand-protein complexes were recorded in kcal/mol.

2.6. Site-Directed in Silico Mutagenesis

The Ligand Docker of CHARMM-GUI (https://www.charmm-gui.org) [35] was used to generate in silico mutants of selected putative RHTs. Default parameters were maintained in the *PDB Manipulation Options* section, except for *Mutation,* where the target amino acid was selected for modification. In the *Grid Generation* section, *Blind Docking* was selected to ensure that the search space fully encompassed the substrate-binding site. For solvation, an orthorhombic TIP3P water box was used with a padding of 10 Å around the protein, and the system was neutralized with KCl ions at a physiological concentration of 0.15 M. The docking environment was set at pH 7.0, and CHARMM36m force fields were applied for energy parameterization. UDP-L-rhamnose assessed which amino acids contributed to binding affinity after the mutation. Docking analyses were performed using the *AutoDock Vina* package.

2.7. Strains and Culture Conditions

Conidia were obtained from *Aspergillus niger* FGSC A732, *Madurella mycetomatis* (Laveran) Brumpt (ATCC 64942), *Metarhizium anisopliae* Xi-18-2, *M. brunneum* EC25, *M. guizhouense* HA11-2 (environmental isolate) [36], *Trichoderma atroviride* IMI 206040 (ATCC 32173), *T. harzianum* T35, *T. reesei* RUTC30 (ATCC 56765), and *T. virens* Tv 29.8. Yeast-like cells were obtained from *S. schenckii*

 doi:10.20944/preprints202505.2096.v1

1099-18 (ATCC MYA 4821), *Candida albicans* SC5314 (ATCC MYA-2876), and *Saccharomyces cerevisiae* BY4741 (ATCC 4040002).

All strains were cultured in YPD medium (1% yeast extract, 2% gelatin peptone, and 3% glucose). Cultures were incubated at 28 °C with shaking at 120 rpm, except for *S. schenckii* and *M. mycetomatis*, which were incubated at 37 °C under the same shaking conditions. *C. albicans* and *S. cerevisiae* were grown for 1 day; *Metarhizium*, *Madurella*, *Sporothrix*, and *Trichoderma* species for 4 days; and *A. niger* for 10 days.

2.8. Analysis of Cell Wall Composition

Conidial and yeast-like cells were pelleted, washed three times with deionized water, and disrupted using a Braun homogenizer (Braun Biotech International GmbH, Melsungen, Germany), as described previously [37,38]. The resulting cell walls were washed by centrifuging and resuspended six times in deionized water. Further purification was performed by serial incubations with SDS, β-mercaptoethanol, 1 mM EDTA (pH 7.5), and 50 mM Tris-HCl buffer to remove intracellular contaminants. As previously reported, samples were hydrolyzed with 2 M trifluoroacetic acid [38].

The acid-hydrolyzed cell wall samples were analyzed by high-performance anion-exchange chromatography with pulsed amperometric detection (HPAEC-PAD) using a Dionex system (Thermo Fisher Scientific, Waltham, MA, USA) under separation conditions like those previously described [37].

2.9. Enzyme Activity

Rhamnosyltransferase activity was analyzed using the supernatant obtained from cell disruption with a Braun homogenizer. For the enzyme assays, 200 ng of α-1,6-mannobiose (Dextra Laboratories, Reading, UK) was used as the rhamnose acceptor, and 500 μM of UDP-L-rhamnose (Chemily Glycoscience, Peachtree Corners, GA, USA) as the donor substrate. Three experimental conditions were established: (i) a complete reaction containing the enzyme, the acceptor, and UDP-L-rhamnose; (ii) a no-acceptor control, in which the reaction was performed only with the enzyme and UDP-L-rhamnose; and (iii) a heat-inactivated enzyme control, in which the complete reaction mixture was subjected to thermal treatment at 50 °C for 60 minutes to inactivate the enzyme. Reactions were carried out in a final volume of 100 μL using a potassium phosphate buffer solution (50 mM, pH 7.0), preincubated at 37 °C for 2 minutes [8]. Reaction products were analyzed by HPAEC-PAD using a Dionex system (Thermo Fisher Scientific) equipped with a CarboPac PA-1 column. Separation conditions were like those previously described for the analysis of cell wall composition [37].

3. Results

3.1. HMM Construction of RHTs and Searches with HMMER

After constructing the HMM profiles for Rht1 and Rht2, searches were performed using the fungal protein database from NCBI. A total of 302 genera were identified for Rht1 and 180 genera for Rht2.

To support the presence of a complete rhamnose biosynthetic pathway, a search for orthologs of the enzyme RmlD was conducted. RmlD is a UDP-4-keto-6-deoxyglucose-3,5-epimerase/-4-reductase responsible for the final step in UDP-L-rhamnose synthesis in *S. schenckii* [35]. Based on this, an HMM profile was constructed, identifying RmlD orthologs in 638 fungal genera. The comparison of RmlD and Rht1 revealed 263 shared genera, accounting for 87.09% of the 302 initial genera for Rht1. Likewise, 172 shared genera were found for Rht2 and RmlD, representing 95.56% of the 180 initially identified genera, suggesting a conserved rhamnose biosynthetic context.

For Rht1, 720 species were identified across 263 genera, while 438 species belonging to 172 genera were obtained for Rht2 (Table 1). The most representative genera for both included *Fusarium*, *Colletotrichum*, *Aspergillus*, *Trichoderma*, and *Claviceps*.

doi:10.20944/preprints202505.2096.v1

Table 1. Genera, species, and accession numbers for putative RHTs.

Genera	Species	Rht1 accession	Rht2 accession	Genera	Species	Rht1 accession	Rht2 accession
Akanthomyces	*Akanthomyces lecanii*	OAA77240.1	OAA70212.1	*Aspergillus*	*Aspergillus luchuensis*	XP_041539789.1	OJZ81278.1
	Akanthomyces muscarius	XP_056049605.1	XP_056054863.1		*Aspergillus mulundensis*	XP_026604170.1	XP_026604105.1
Alectoria	*Alectoria fallacina*	CAF9938699.1	CAF9943470.1		*Aspergillus neoniger*	XP_025476319.1	XP_025484262.1
	Alectoria sarmentosa	CAD6567071.1	CAD6566374.1		*Aspergillus niger*	EHA26758.1	GKZ64237.1
Annulohypoxylon	*Annulohypoxylon bovei*	KAI2473205.1	KAI2463407.1		*Aspergillus piperis*	XP_025512668.1	XP_025513870.1
	Annulohypoxylon moriforme	KAI1454471.1	KAI1454171.1		*Aspergillus sclerotiicarbonarius*	PYI12272.1	PYI02360.1
	Annulohypoxylon nitens	KAI0892314.1	KAI0896334.1		*Aspergillus sclerotioniger*	XP_025471984.1	XP_025463962.1
	Annulohypoxylon stygium	KAI1446163.1	KAI1445084.1		*Aspergillus tubingensis*	XP_035356720.1	GLB04893.1
	Annulohypoxylon truncatum	XP_047856260.1	XP_047849137.1		*Aspergillus versicolor*	XP_040664242.1	UZP48228.1
Aphanocladium	*Aphanocladium album*	KAJ6785788.1	KAJ6789860.1		*Aspergillus welwitschiae*	XP_026629939.1	XP_026624638.1
Apiosordaria	*Apiosordaria backusii*	KAK0701482.1	KAK0718985.1	*Aureobasidium*	*Aureobasidium melanogenum*	XP_040877796.1	KAG9597102.1
Ascochyta	*Ascochyta clinopodiicola*	KAJ4351106.1	KAJ4346241.1	*Beauveria*	*Beauveria bassiana*	XP_008598136.1	XP_008602005.1
	Ascochyta lentis	KAF9700101.1	KAF9695519.1		*Beauveria brongniartii*	OAA37782.1	OAA39919.1
	Ascochyta rabiei	XP_059492683.1	XP_038797369.2	*Bipolaris*	*Bipolaris maydis*	XP_014081052.1	XP_014078238.1
Aspergillus	*Aspergillus awamori*	GCB26403.1	GCB23152.1		*Bipolaris oryzae*	XP_007689746.1	XP_007682054.1
	Aspergillus brasiliensis	OJJ74616.1	GKZ22376.1	*Biscogniauxia*	*Biscogniauxia marginata*	KAI1502855.1	KAI1498195.1
	Aspergillus carbonarius	OOF95088.1	OOG00364.1		*Biscogniauxia mediterranea*	KAI1491791.1	KAI1491404.1
	Aspergillus carlsbadensis	KAJ0426393.1	KAJ0415219.1	*Boeremia*	*Boeremia exigua*	KAJ8115054.1	XP_046000075.1
	Aspergillus costaricensis	XP_025534806.1	XP_025540426.1	*Botryosphaeria*	*Botryosphaeria dothidea*	KAF4303495.1	KAF4305872.1
	Aspergillus eucalypticola	XP_025389724.1	XP_025383912.1	*Botryotinia*	*Botryotinia calthae*	TEY39080.1	TEY37428.1
	Aspergillus hancockii	KAF7593079.1	KAF7587272.1		*Botryotinia convoluta*	TGO61616.1	TGO51629.1
	Aspergillus homomorphus	XP_025547265.1	XP_025552456.1		*Botryotinia globosa*	KAF7896435.1	KAF7901251.1
	Aspergillus ibericus	XP_025575496.1	XP_025578007.1		*Botryotinia narcissicola*	TGO69167.1	TGO56301.1
Botrytis	*Botrytis aclada*	KAF7946254.1	KAF7956861.1	*Claviceps*	*Claviceps maximensis*	KAG6000611.1	KAG6002038.1
	Botrytis byssoidea	XP_038729320.1	XP_038733006.1		*Claviceps monticola*	KAG5947883.1	KAG5944898.1
	Botrytis cinerea	XP_001557717.1	EMR81961.1		*Claviceps purpurea*	KAG6139429.1	KAG6132685.1
	Botrytis deweyae	XP_038812155.1	XP_038811764.1		*Claviceps pusilla*	KAG6000469.1	KAG5989301.1
	Botrytis fragariae	XP_037188780.1	XP_037193260.1		*Claviceps sorghi*	KAG5929518.1	KAG5949601.1
	Botrytis galanthina	THV55011.1	THV45154.1		*Claviceps spartinae*	KAG5989744.1	KAG5994791.1
	Botrytis paeoniae	TGO28479.1	TGO20471.1	*Clohesyomyces*	*Clohesyomyces aquaticus*	ORX91671.1	ORY16921.1
	Botrytis porri	XP_038770654.1	XP_038768623.1	*Clonostachys*	*Clonostachys byssicola*	CAG9999494.1	CAG9995431.1
	Botrytis sinoallii	XP_038758083.1	XP_038760845.1		*Clonostachys chloroleuca*	CAI6100125.1	CAI6093753.1
	Botrytis tulipae	TGO11019.1	TGO09160.1		*Clonostachys rhizophaga*	CAH0016028.1	CAH0019948.1
Byssothecium	*Byssothecium circinans*	KAF1950910.1	KAF1948264.1		*Clonostachys rosea*	CAG9943511.1	CAG9952845.1
Cephalotrichum	*Cephalotrichum gorgonifer*	SPN99558.1	SPO03607.1		*Clonostachys solani*	CAH0053102.1	CAH0038538.1
Cercophora	*Cercophora newfieldiana*	KAK0644497.1	KAK0638609.1	*Collariella*	*Collariella sp.*	KAJ4302561.1	KAJ4286560.1
	Cercophora samala	KAK0666350.1	KAK0667676.1	*Colletotrichum*	*Colletotrichum abscissum*	KAI3548229.1	KAI3530008.1
Cladophialophora	*Cladophialophora carrionii*	XP_008726825.1	XP_008725802.1		*Colletotrichum acutatum*	KAK1728796.1	KAK1724125.1

 doi:10.20944/preprints202505.2096.v1

	Cladophialophora chaetospira	KAJ9603522.1	KAJ9615145.1
Claussenomyces	*Claussenomyces sp.*	KAI9740875.1	KAI9732059.1
Claviceps	*Claviceps africana*	KAG5920846.1	KAG5919883.1
	Claviceps arundinis	KAG5952815.1	KAG5966788.1
	Claviceps capensis	KAG5921672.1	KAG5921632.1
	Claviceps cyperi	KAG5952799.1	KAG5965626.1
	Claviceps digitariae	KAG5972007.1	KAG5982393.1
	Claviceps humidiphila	KAG6112056.1	KAG6118839.1
	Claviceps lovelessii	KAG5991086.1	KAG5986980.1
Colletotrichum	*Colletotrichum filicis*	KAI3546144.1	KAI3528431.1
	Colletotrichum fioriniae	XP_053047741.1	KAJ0331578.1
	Colletotrichum fructicola	KAF4889272.1	XP_031878303.1
	Colletotrichum gloeosporioides	KAH9228900.1	KAH9225977.1
	Colletotrichum godetiae	KAK1688763.1	KAK1657259.1
	Colletotrichum graminicola	XP_008092350.1	XP_008100482.1
	Colletotrichum higginsianum	XP_018156347.1	GJC91227.1
	Colletotrichum incanum	KZL82890.1	OHW97533.1
	Colletotrichum karsti	XP_038751836.1	XP_038743776.1
	Colletotrichum limetticola	KAK0377708.1	KAK0371775.1
	Colletotrichum liriopes	GJC85203.1	GJC77217.1
	Colletotrichum lupini	KAK1717078.1	KAK1705670.1
	Colletotrichum musicola	KAF6844777.1	KAF6838802.1
	Colletotrichum navitas	KAK1589649.1	KAK1573862.1
	Colletotrichum noveboracense	KAJ0291777.1	KAJ0277668.1
	Colletotrichum nupharicola	KAJ0294167.1	KAJ0337848.1
	Colletotrichum nymphaeae	KXH63825.1	KXH45981.1
	Colletotrichum orbiculare	TDZ14397.1	TDZ14673.1
	Colletotrichum orchidophilum	XP_022472465.1	XP_022475743.1
	Colletotrichum paranaense	KAK1543004.1	KAK1540822.1
	Colletotrichum phormii	KAK1654730.1	KAK1635646.1
	Colletotrichum plurivorum	KAF6839083.1	KAF6829629.1
	Colletotrichum salicis	KXH68169.1	KXH39943.1
Cordyceps	*Cordyceps militaris*	ATY63072.1	XP_006674754.1
Cryphonectria	*Cryphonectria parasitica*	XP_040771798.1	XP_040776216.1
Cucurbitaria	*Cucurbitaria berberidis*	XP_040787765.1	XP_040790731.1
Cytospora	*Cytospora leucostoma*	ROW08189.1	ROW16112.1
Dactylonectria	*Dactylonectria estremocensis*	KAH7149514.1	KAH7159663.1
	Dactylonectria macrodidyma	KAH7148757.1	KAH7143671.1
Daldinia	*Daldinia bambusicola*	KAI1806735.1	KAI1805383.1
	Daldinia caldariorum	XP_047790272.1	XP_047785741.1
	Daldinia childiae	XP_033434965.1	XP_033438607.1
Colletotrichum	*Colletotrichum aenigma*	XP_037173265.1	XP_037184972.1
	Colletotrichum asianum	KAF0316491.1	KAF0316378.1
	Colletotrichum camelliae	KAH0426174.1	KAH0442418.1
	Colletotrichum caudatum	KAK2056574.1	KAK2059483.1
	Colletotrichum cereale	KAK1983501.1	KAK1986054.1
	Colletotrichum chlorophyti	OLN82217.1	OLN96240.1
	Colletotrichum chrysophilum	KAK1850901.1	XP_053034241.1
	Colletotrichum eremochloae	KAK2012662.1	KAK2005828.1
	Colletotrichum falcatum	KAK1997804.1	KAK1994865.1
	Colletotrichum scovillei	XP_035338834.1	XP_035327966.1
	Colletotrichum shisoi	TQN74967.1	TQN67810.1
	Colletotrichum siamense	XP_036489658.1	KAF4814982.1
	Colletotrichum sidae	TEA14001.1	TEA21432.1
	Colletotrichum simmondsii	KXH39862.1	KXH40793.1
	Colletotrichum sojae	KAF6819562.1	KAF6806549.1
	Colletotrichum somersetense	KAK2040239.1	KAK2043394.1
	Colletotrichum sublineola	KAK1967522.1	KDN67295.1
	Colletotrichum tamarilloi	KAK1504719.1	KAK1490332.1
	Colletotrichum tanaceti	KAJ0168474.1	KAJ0162061.1
	Colletotrichum tofieldiae	GKT60742.1	KZL66573.1
	Colletotrichum trifolii	TDZ55051.1	TDZ54034.1
	Colletotrichum tropicale	KAJ3960067.1	KAJ3960792.1
	Colletotrichum truncatum	XP_036584982.1	XP_036576291.1
	Colletotrichum viniferum	KAF4928949.1	KAF4925869.1
	Colletotrichum zoysiae	KAK2027693.1	KAK2035655.1
Coniella	*Coniella lustricola*	PSR99022.1	PSR88517.1
Coniochaeta	*Coniochaeta hoffmannii*	KAJ9161119.1	KAJ9155879.1
	Coniochaeta ligniaria	OIW29085.1	OIW23813.1
	Coniochaeta pulveracea	RKU46626.1	RKU48537.1
Conoideocrella	*Conoideocrella luteorostrata*	KAK2612324.1	KAK2616729.1
Cordyceps	*Cordyceps fumosorosea*	XP_018701293.1	XP_018701796.1
	Cordyceps javanica	TQV92045.1	TQV95450.1
Durotheca	*Durotheca rogersii*	XP_051368855.1	XP_051373960.1
Echria	*Echria macrotheca*	KAK1750845.1	KAK1751134.1
Emericellopsis	*Emericellopsis atlantica*	XP_046118537.1	XP_046121130.1
Epichloe	*Epichloe festucae*	QPH04205.1	QPH11511.1
Epicoccum	*Epicoccum nigrum*	KAG9204943.1	OSS46826.1
Escovopsis	*Escovopsis weberi*	KOS20329.1	KOS17718.1
Eutypa	*Eutypa lata*	KAI1250716.1	EMR68577.1
Fusarium	*Fusarium acutatum*	KAF4417706.1	KAF4435765.1
	Fusarium albosuccineum	KAF4453631.1	KAF4470643.1

 doi:10.20944/preprints202505.2096.v1

	Daldinia decipiens	XP_049104523.1	XP_049095979.1
	Daldinia eschscholtzii	KAI1473488.1	KAI1475320.1
	Daldinia grandis	KAI0108307.1	KAI0095932.1
	Daldinia loculata	KAI2779756.1	KAI2777984.1
	Daldinia vernicosa	XP_047867275.1	XP_047863139.1
Decorospora	*Decorospora gaudefroyi*	KAF1831972.1	KAF1836052.1
Dendryphion	*Dendryphion nanum*	KAH7135752.1	KAH7135333.1
Diaporthe	*Diaporthe ampelina*	KKY39506.1	KKY35200.1
	Diaporthe amygdali	KAK2615727.1	XP_052998701.1
	Diaporthe batatas	XP_044649453.1	XP_044648057.1
	Diaporthe eres	KAI7784925.1	KAI7784403.1
	Diaporthe helianthi	POS75403.1	POS81165.1
	Diaporthe ilicicola	KAI3397926.1	KAI3399409.1
Didymella	*Didymella heteroderae*	KAF3044419.1	KAF3045961.1
	Didymella pomorum	KAJ4403697.1	KAJ4411464.1
Fusarium	*Fusarium flagelliforme*	XP_045987014.1	XP_045981550.1
	Fusarium floridanum	RSL77313.1	RSL81449.1
	Fusarium fujikuroi	KLO94116.1	KLO93232.1
	Fusarium gaditjirri	KAF4952308.1	KAF4947967.1
	Fusarium graminearum	XP_011318866.1	PCD36796.1
	Fusarium graminum	KAF4989143.1	KAF4992880.1
	Fusarium heterosporum	KAF5673296.1	KAF5665361.1
	Fusarium irregulare	KAJ4028622.1	KAJ4002951.1
	Fusarium keratoplasticum	XP_052913386.1	XP_052910685.1
	Fusarium kuroshium	RMJ06590.1	RMJ08909.1
	Fusarium langsethiae	GKU13606.1	KPA39552.1
	Fusarium longipes	RGP64061.1	RGP64175.1
	Fusarium mangiferae	XP_041681908.1	XP_041689374.1
	Fusarium mundagurra	KAF5703820.1	KAF5715773.1
	Fusarium musae	XP_044681754.1	XP_044678177.1
	Fusarium napiforme	KAF5543507.1	KAF5530306.1
	Fusarium odoratissimum	XP_031063514.1	XP_031068097.1
	Fusarium oligoseptatum	RSM10484.1	RSM09688.1
	Fusarium oxysporum	RKK72986.1	KAJ4047383.1
	Fusarium piperis	KAJ4307910.1	KAJ4328312.1
	Fusarium poae	XP_044713521.1	OBS22433.1
	Fusarium proliferatum	KAI1009795.1	KAG4256852.1
	Fusarium pseudoanthophilum	KAF5579641.1	KAF5585516.1
Hypoxylon	*Hypoxylon crocopeplum*	KAI1380815.1	KAI1377137.1
	Hypoxylon fragiforme	XP_049114466.1	XP_049117066.1
	Hypoxylon fuscum	KAI1401401.1	KAI1399455.1
	Hypoxylon rubiginosum	KAI4863860.1	KAI4864951.1
Fusarium	*Fusarium ambrosium*	RSM11772.1	RSL97308.1
	Fusarium austroafricanum	KAF4446928.1	KAF4445897.1
	Fusarium austroamericanum	KAF5236077.1	KAF5233753.1
	Fusarium avenaceum	KAH6968718.1	KIL89965.1
	Fusarium beomiforme	KAF4344697.1	KAF4334837.1
	Fusarium chuoi	KAI1013357.1	KAI1019319.1
	Fusarium coffeatum	XP_031013799.1	XP_031011366.1
	Fusarium coicis	KAF5967328.1	KAF5967796.1
	Fusarium culmorum	PTD03166.1	PTD08619.1
	Fusarium decemcellulare	KAF5000569.1	KAF4990227.1
	Fusarium denticulatum	KAF5669558.1	KAF5676768.1
	Fusarium duplospermum	RSL50528.1	RSL66332.1
	Fusarium equiseti	CAG7560528.1	CAG7554771.1
	Fusarium euwallaceae	RTE71192.1	RTE70560.1
	Fusarium falciforme	XP_053008353.1	KAJ4142701.1
	Fusarium pseudocircinatum	KAF5593813.1	KAF5606259.1
	Fusarium pseudograminearum	QPC77377.1	QPC79958.1
	Fusarium redolens	XP_046051426.1	XP_046045510.1
	Fusarium sarcochroum	KAF4970797.1	KAF4970128.1
	Fusarium solani	XP_046134246.1	XP_046129193.1
	Fusarium solani-melongenae	UPL01582.1	UPL00732.1
	Fusarium sporotrichioides	RGP74396.1	RGP62770.1
	Fusarium tjaetaba	XP_037201359.1	XP_037210905.1
	Fusarium tricinctum	KAH7262271.1	KAH7263618.1
	Fusarium vanettenii	XP_003051169.1	XP_003048134.1
	Fusarium venenatum	XP_025590567.1	KAG8361315.1
	Fusarium verticillioides	XP_018746363.1	XP_018759284.1
	Fusarium xylarioides	KAG5745984.1	KAG5750058.1
	Fusarium zealandicum	KAF4977827.1	KAF4976478.1
Gaeumannomyces	*Gaeumannomyces tritici*	XP_009216301.1	XP_009229452.1
Glonium	*Glonium stellatum*	OCL07134.1	OCL02246.1
Gnomoniopsis	*Gnomoniopsis smithogilvyi*	KAJ4396492.1	KAJ4397375.1
Hapsidospora	*Hapsidospora chrysogena*	KFH41691.1	KFH48365.1
Hirsutella	*Hirsutella minnesotensis*	KJZ78224.1	KJZ71824.1
	Hirsutella rhossiliensis	XP_044715856.1	XP_044720357.1
Hypomontagnella	*Hypomontagnella monticulosa*	KAI0386569.1	KAI0378476.1
	Hypomontagnella submonticulosa	KAI2638882.1	KAI2620953.1
Hypoxylon	*Hypoxylon cercidicola*	KAI1778259.1	KAI1774420.1
Melanomma	*Melanomma pulvis-pyrius*	KAF2800153.1	KAF2786108.1
Metarhizium	*Metarhizium acridum*	XP_007810202.1	KAG8422976.1
	Metarhizium album	XP_040678038.1	XP_040683175.1
	Metarhizium anisopliae	KJK84664.1	KJK80520.1

 doi:10.20944/preprints202505.2096.v1

Ilyonectria	*Ilyonectria destructans*	KAH7011765.1	KAH7002281.1		*Metarhizium brunneum*	XP_014545532.1	XP_014548452.1
	Ilyonectria robusta	XP_046104787.1	XP_046110074.1		Metarhizium guizhouense	KID87172.1	KID92007.1
Immersiella	*Immersiella caudata*	KAK0616255.1	KAK0624188.1		*Metarhizium humberi*	KAH0599959.1	KAH0597174.1
Jackrogersella	*Jackrogersella minutella*	KAI1107063.1	KAI1099809.1		*Metarhizium rileyi*	OAA42134.1	OAA43280.1
Kalmusia	*Kalmusia sp.*	KAJ4295449.1	KAJ4293461.1		*Metarhizium robertsii*	XP_007819142.2	XP_007822448.1
Karstenula	*Karstenula rhodostoma*	KAF2449100.1	KAF2448746.1	*Microdochium*	*Microdochium bolleyi*	KXJ90972.1	KXJ92914.1
Lasallia	*Lasallia pustulata*	KAA6414625.1	KAA6413478.1		*Microdochium nivale*	KAJ1326562.1	KAJ1329274.1
Lasiosphaeria	*Lasiosphaeria miniovina*	KAK0733273.1	KAK0706185.1		*Microdochium trichocladiopsis*	XP_046009150.1	XP_046013910.1
Lecanicillium	*Lecanicillium saksenae*	KAJ3498506.1	KAJ3497866.1	*Moelleriella*	*Moelleriella libera*	OAA33830.1	KZZ90826.1
Leptographium	*Leptographium clavigerum*	XP_014168710.1	XP_014175810.1	*Monilinia*	*Monilinia laxa*	KAB8300938.1	KAB8303359.1
Lophiostoma	*Lophiostoma macrostomum*	KAF2657876.1	KAF2648898.1	*Monosporascus*	*Monosporascus cannonballus*	RYO83116.1	RYO94743.1
Lophiotrema	*Lophiotrema nucula*	KAF2116133.1	KAF2113514.1		*Monosporascus ibericus*	RYP07719.1	RYP11091.1
Lophium	*Lophium mytilinum*	KAF2488524.1	KAF2497128.1	*Mytilinidion*	*Mytilinidion resinicola*	XP_033579010.1	XP_033568734.1
Macrophomina	*Macrophomina phaseolina*	EKG10336.1	EKG11414.1	*Neofusicoccum*	*Neofusicoccum parvum*	EOD43149.1	EOD53031.1
Macroventuria	*Macroventuria anomochaeta*	XP_033560458.1	XP_033560487.1	*Neonectria*	*Neonectria ditissima*	KPM46246.1	KPM40292.1
Madurella	*Madurella mycetomatis*	KXX75366.1	KXX79238.1	*Niveomyces*	*Niveomyces insectorum*	AZHD01000039.1	OAA57048.1
Magnaporthiopsis	*Magnaporthiopsis poae*	KLU92256.1	KLU84765.1	*Ophiocordyceps*	*Ophiocordyceps sinensis*	KAF4508004.1	EQK98407.1
Mariannaea	*Mariannaea sp.*	KAI5462524.1	KAI5458596.1	*Ophiostoma*	*Ophiostoma piceae*	EPE10043.1	EPE10437.1
Massarina	*Massarina eburnea*	KAF2642528.1	KAF2646682.1	*Paraphoma*	*Paraphoma chrysanthemicola*	KAH7083038.1	KAH7071542.1
Penicilliopsis	*Penicilliopsis zonata*	XP_022583757.1	XP_022577075.1	*Rhexocercosporidium*	*Rhexocercosporidium sp.*	KAH7350870.1	KAH7346361.1
Penicillium	*Penicillium alfredii*	XP_056508930.1	XP_056509782.1	*Rostrohypoxylon*	*Rostrohypoxylon terebratum*	KAI1092632.1	KAI1090772.1
	Penicillium bovifimosum	XP_056523126.1	XP_056526610.1	*Sclerotinia*	*Sclerotinia borealis*	ESZ92680.1	ESZ95592.1
	Penicillium macrosclerotiorum	XP_056932270.1	XP_056934836.1		*Sclerotinia nivalis*	KAJ8059674.1	KAJ8071588.1
	Penicillium odoratum	XP_057001022.1	XP_057000407.1		*Sclerotinia sclerotiorum*	XP_001588350.1	XP_001589362.1
Periconia	*Periconia macrospinosa*	PVI05090.1	PVH96591.1		*Sclerotinia trifoliorum*	CAD6445273.1	CAD6453695.1
Pestalotiopsis	*Pestalotiopsis fici*	XP_007834024.1	XP_007841187.1	*Setomelanomma*	*Setomelanomma holmii*	KAF2025903.1	KAF2023082.1
Phaeoacremonium	*Phaeoacremonium minimum*	XP_007914921.1	XP_007916963.1	*Sodiomyces*	*Sodiomyces alkalinus*	XP_028463447.1	XP_028465600.1
Phaeomoniella	*Phaeomoniella chlamydospora*	KKY25069.1	KKY20074.1	*Sporothrix*	*Sporothrix brasiliensis*	XP_040616120.1	XP_040617365.1
Phialemonium	*Phialemonium atrogriseum*	KAK1762406.1	KAK1762806.1		*Sporothrix schenckii*	XP_016583713.1	XP_016584143.1
Pleurostoma	*Pleurostoma richardsiae*	KAJ9156358.1	KAJ9149742.1	*Stachybotrys*	*Stachybotrys chartarum*	KFA52060.1	KFA76153.1
Podospora	*Podospora anserina*	XP_001903917.1	XP_001904848.1		*Stachybotrys chlorohalonata*	KFA66408.1	KFA67805.1
Polyplosphaeria	*Polyplosphaeria fusca*	KAF2739724.1	KAF2731913.1		*Stachybotrys elegans*	KAH7326028.1	KAH7322735.1
Pseudogymnoascus	*Pseudogymnoascus destructans*	XP_024324285.1	XP_024325152.1	*Stagonospora*	*Stagonospora sp. SRC1lsM3a*	OAL06240.1	OAL04400.1
	Pseudogymnoascus verrucosus	XP_018130987.1	XP_018126712.1	*Staphylotrichum*	*Staphylotrichum longicolle*	KAG7286337.1	KAG7294653.1
Pseudomassariella	*Pseudomassariella vexata*	XP_040716094.1	XP_040718474.1	*Stromatinia*	*Stromatinia cepivora*	KAF7858421.1	KAF7872547.1
Purpureocillium	*Purpureocillium lavendulum*	KAJ6440404.1	KAJ6441125.1	*Stylonectria*	*Stylonectria norvegica*	KAF7554195.1	KAF7554329.1
Purpureocillium	*Purpureocillium lilacinum*	XP_018175438.1	XP_018181559.1	*Talaromyces*	*Talaromyces amestolkiae*	XP_040733191.1	XP_040736898.1
	Purpureocillium takamizusanense	XP_047844175.1	XP_047841106.1		*Talaromyces atroroseus*	XP_020124160.1	XP_020121501.1
Pycnora	*Pycnora praestabilis*	KAI9813616.1	KAI9822666.1	*Thermochaetoides*	*Thermochaetoides thermophila*	XP_006694985.1	XP_006692471.1
Pyrenochaeta	*Pyrenochaeta sp.*	OAL53857.1	OAL46984.1	*Thermothielavioides*	*Thermothielavioides terrestris*	XP_003650890.1	XP_003658264.1
Pyricularia	*Pyricularia grisea*	KAI6356710.1	KAI6379156.1	*Thozetella*	*Thozetella sp.*	KAH8887751.1	KAH8901217.1
	Pyricularia oryzae	KAH8839881.1	KAI6251849.1	*Thyridium*	*Thyridium curvatum*	XP_030997551.1	XP_030999529.1

 doi:10.20944/preprints202505.2096.v1

Tolypocladium	*Tolypocladium ophioglossoides*	KND89648.1	KND93039.1
	Tolypocladium paradoxum	POR38644.1	POR35566.1
Trematosphaeria	*Trematosphaeria pertusa*	XP_033678715.1	XP_033681098.1
Trichoderma	*Trichoderma arundinaceum*	RFU72470.1	RFU78995.1
	Trichoderma asperelloides	KAH8130780.1	KAH8127233.1
	Trichoderma asperellum	XP_024758558.1	UKZ86906.1
	Trichoderma atroviride	XP_013943227.1	UKZ67550.1
	Trichoderma breve	XP_056025069.1	XP_056030790.1
	Trichoderma citrinoviride	XP_024751380.1	XP_024752346.1
	Trichoderma cornu-damae	KAH6609697.1	KAH6605774.1
	Trichoderma gracile	KAH0495172.1	KAH0492740.1
	Trichoderma guizhouense	OPB40233.1	OPB36448.1
	Trichoderma harzianum	XP_024772549.1	KKO97596.1
	Trichoderma longibrachiatum	PTB74489.1	PTB77621.1
	Trichoderma reesei	XP_006961478.1	XP_006968899.1
	Trichoderma semiorbis	KAH0522488.1	KAH0529301.1
	Trichoderma simmonsii	QYT05558.1	QYS95815.1
	Trichoderma virens	XP_013961374.1	XP_013957984.1
Trichothecium	*Trichothecium roseum*	KAI9900351.1	KAI9901541.1
Truncatella	*Truncatella angustata*	XP_045959758.1	KAH8199344.1
Ustilaginoidea	*Ustilaginoidea virens*	XP_043000764.1	XP_042995238.1
Valsa	*Valsa sordida*	ROV96478.1	ROV93292.1
Whalleya	*Whalleya microplaca*	KAI1081251.1	KAI1080707.1
Xylona	*Xylona heveae*	XP_018185144.1	XP_018185306.1
Zopfia	*Zopfia rhizophila*	KAF2193744.1	KAF2191997.1

Accession: A unique identifier assigned to each biological sequence within the NCBI database.

 doi:10.20944/preprints202505.2096.v1

3.2. Phylogenetic Distribution of Putative RHTs

The phylogenetic analysis of the putative RHTs sequences was performed using the PhyML 3.0 platform, employing the maximum likelihood method with branch support based on the aLRT SH-like approximation. The resulting phylogenetic trees were compared to the taxonomic classification of the analyzed fungal species to identify congruent patterns that support the evolutionary relationships of the candidate RHTs. Several clades with high evolutionary relatedness were identified in both analyses and were highlighted using colored boxes to facilitate interpretation.

For Rht1, similarities were observed between the phylogeny and taxonomic classification. For instance, species of the genus *Sporothrix* grouped into a clade alongside representatives of the genera *Ophiostoma* and *Pycularia* (Blue Box), which is consistent with previous studies indicating a phylogenetic relationship between *Sporothrix* and *Ophiostoma*, both members of the Ophiostomataceae family. Nearby, *Magnaporthiopsis* and *Gaeumannomyces* (Yellow Box) also clustered consistent with their shared membership in the order Magnaporthales. In another clade (Green Box), the genera *Eutypa*, *Biscogniauxia*, *Monosporascus*, and *Microdochium* exhibited similar distribution patterns in both trees. The placement of *Echiria*, *Immersiella*, *Thermothielavioides*, and *Madurella* within the phylogenetic tree (Orange Box) indicated that these genera generally cluster within the same clade, despite minor internal rearrangements. Additionally, the genera *Phaeoacremonium* and *Coniochaeta* showed consistent groupings in the phylogenetic and taxonomic trees, suggesting congruence between their genetic evolution and taxonomic classification. A comparative view of the Rht1 phylogenetic (left) and taxonomic (right) trees is presented in Figure 1.

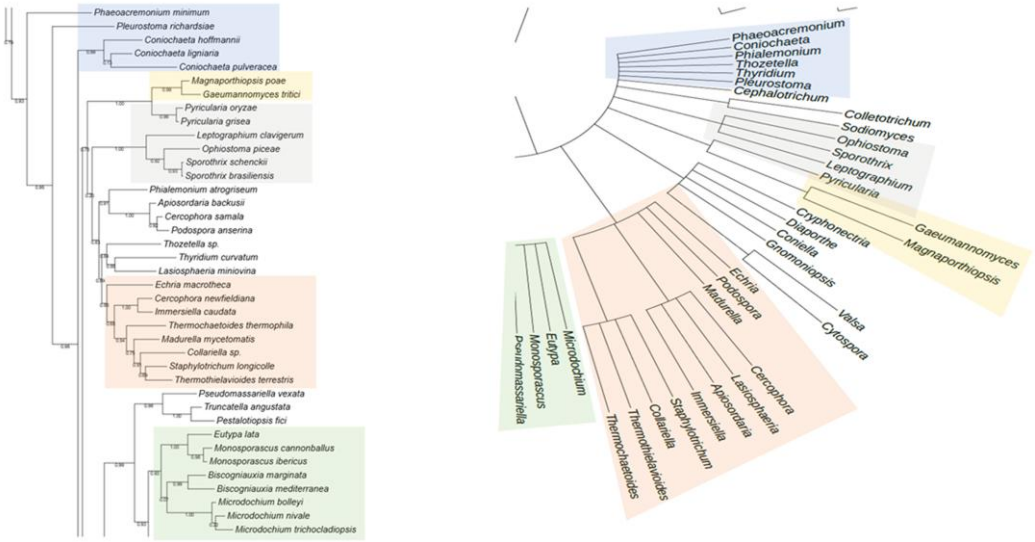

Figure 1. Comparison between the phylogenetic distribution of Rht1 (left) and the corresponding taxonomic tree (right). Areas highlighted with the same color indicate similarities in the grouping of genera across both trees.

For Rht2, numerous correspondences were observed between phylogeny and taxonomy across various groups. A clear conservation was noted in the clade comprising *Sporothrix*, *Ophiostoma*, and *Colletotrichum* (Blue Box), which clustered similarly in both trees. Likewise, *Magnaporthiopsis* and *Diaporthe* (Yellow Box) retained a consistent organization, in agreement with their classification within the class Sordariomycetes. In the Green Box, *Purpureocillium*, *Tolypocladium*, and *Trichoderma* were grouped similarly in both analyses. Similarly, in the Orange Box, the genera *Neonectria*, *Fusarium*, and *Dactylonectria* formed the same clade in both trees. Overall, the comparison of phylogenetic and taxonomic trees for Rht2 revealed a high degree of concordance, suggesting that the evolutionary history of these sequences aligns with the current taxonomic framework. A side-by-side view of the Rht2 phylogenetic (left) and taxonomic (right) trees is shown in Figure 2.

 doi:10.20944/preprints202505.2096.v1

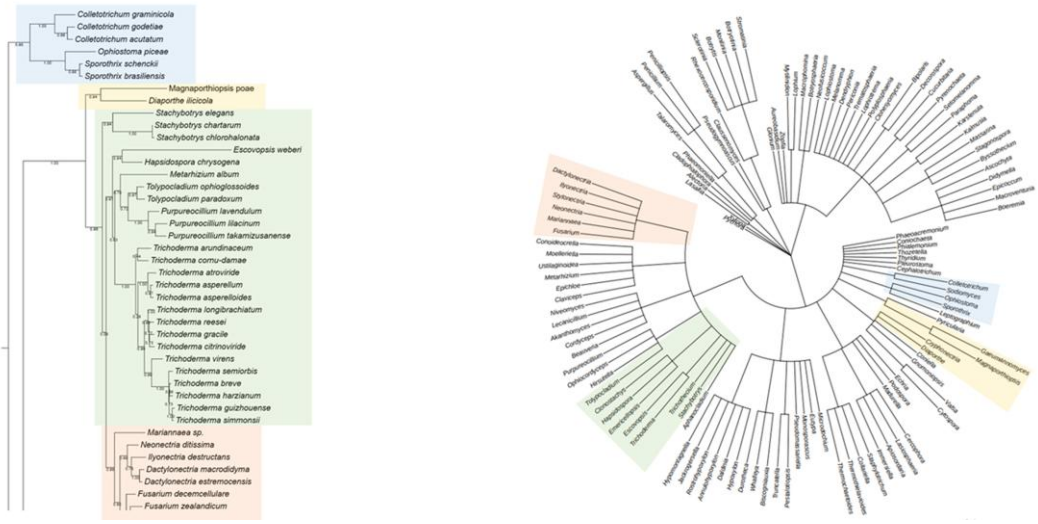

Figure 2. Comparison between the phylogenetic distribution of Rht2 (left) and the corresponding taxonomic tree (right). Areas highlighted with the same color indicate similarities in the grouping of genera across both trees.

3.2. Identification and Distribution of Conserved Motifs in Putative RHTs

The identification and distribution of conserved motifs in putative RHTs were analyzed using MEME Suite, based on protein sequences obtained from HMMER searches (Table 2). For the Rht1 motif analysis, 351 protein sequences were analyzed, with lengths ranging from 159 to 720 amino acids and an average length of 233 amino acids. Five conserved motifs were identified in putative Rht1 sequences. Motif 1, TXGATXXF (where "X" represents any amino acid), was detected in 99.4% of the sequences. Motif 2, LXXQXGXX, was found in 100%, while the motif 3, HAGXGXI, appeared in 95.4% of sequences. The motif 4, XVPNXXLXXXHQ, was also present in 100%, and the motif 5, EXAXXXXXXGYX, in 94.5%. Motif logos are shown in Figure 3A.

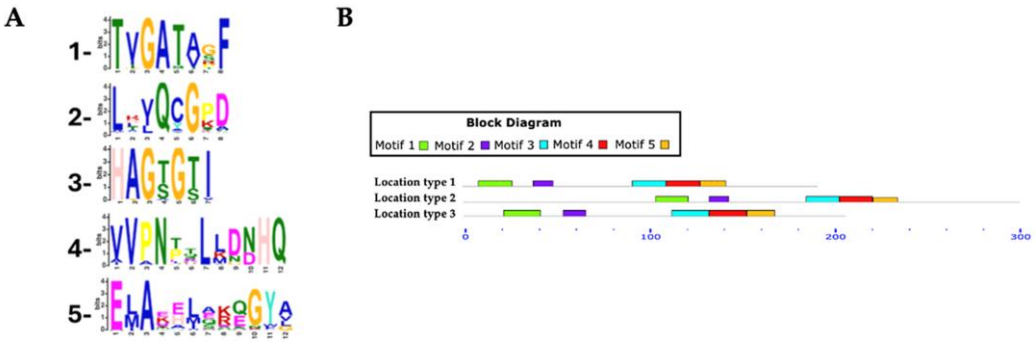

Figure 3. Conserved motifs in Rht1 putative sequences. (**A**) Sequence logos of conserved motifs. (**B**) Distribution patterns of motifs in putative Rht1 sequences according to the MAST map.

Among the identified motifs, motif 1 (TXGATXXF) was the most consistently conserved across all genera analyzed, including *Aspergillus*, *Fusarium*, *Colletotrichum*, *Claviceps*, *Trichoderma*, and *Botrytis*. Motif 3 (HAGXGXI) appeared in all *Fusarium* (54), *Claviceps* (13), and *Diaporthe* (6) sequences, as well as in 7 of 8 *Metarhizium*, 14 of 15 *Trichoderma*, and 44 of 50 *Colletotrichum* species.

Most predicted motifs found to start between amino acid positions 1 to 20 (*location type 1*), with 311 sequences initiating in this region, representing 88.60% of the total. In contrast, fewer sequences started between positions 50 to 520 (*location type* 2, 7.12%), and only 15 sequences were located between positions 21 to 50 (*location type* 3, 4.27%).

 doi:10.20944/preprints202505.2096.v1

In terms of motif conservation, some sequences lacked specific motifs: one sequence did not include motif 1, another lacked motif 3, a third lacked motif 4, and 52 sequences did not contain motif 5.

The three motif location types are shown in Figure 3B, while a detailed list of predicted motifs and their respective starting positions across all putative Rht1 sequences can be found in Supplementary Materials (Table S1 and Figure S2).

For Rht2 motif analysis, a total of 351 protein sequences were analyzed, with lengths ranging from 320 to 695 amino acids and an average length of 458 amino acids. Five conserved motifs were identified in putative Rht2 sequences. Motif 1, XQGTXXXX, was detected in 97.1% of the sequences. Motif 2, XXNXXXXXXXPY, was found in 96%, while motif 3, XNXGYGXXXX, appeared in all sequences. Motif 4, VPXXXXGXXXDK, was present in 97.7%, and motif 5, RXXXXGXXXXLX, in 92.3%. Motif logos are shown in Figure 4A.

Among the motifs identified for Rht2, motif 1 (XQGTXXXX) was the most conserved, being present in all analyzed species of *Diaporthe* (6), *Daldinia* (8), *Botrytis* (10), *Claviceps* (13), *Trichoderma* (15), *Fusarium* (54), as well as in 7 out of 8 of *Metarhizium* species, 18 of 19 of *Aspergillus* species, and 49 of 50 of *Colletotrichum* species. Meanwhile, motif 3 (XNXGYGXXXX) was found in all protein sequences from *Metarhizium* (8), *Botrytis* (10), *Trichoderma* (15), and *Fusarium* (54), as well as in 12 out of 13 *Claviceps* species, 17 out of 19 *Aspergillus* species, and 46 out of 50 *Colletotrichum* species.

Most predicted motifs start between amino acid positions 240 to 320 (*location type 1*), with 333 sequences falling within this region, representing 94.87% of the total. In smaller proportions, 15 sequences were identified between positions 321 to 441 (*location type 2*, 4.27%), and only 3 sequences between positions 155 to 239 (*location type 3*, 0.85%).

Regarding the conserved motifs, several sequences were found to lack specific motifs: three sequences did not contain motif 1, two sequences lacked motif 3, another two sequences lacked motif 4, and six sequences did not present motif 5.

The different location types mentioned are illustrated in Figure 4B, while the predicted motifs and their respective positions across all Rht2 putative sequences are provided in Supplementary Materials (Table S3 and Figure S4).

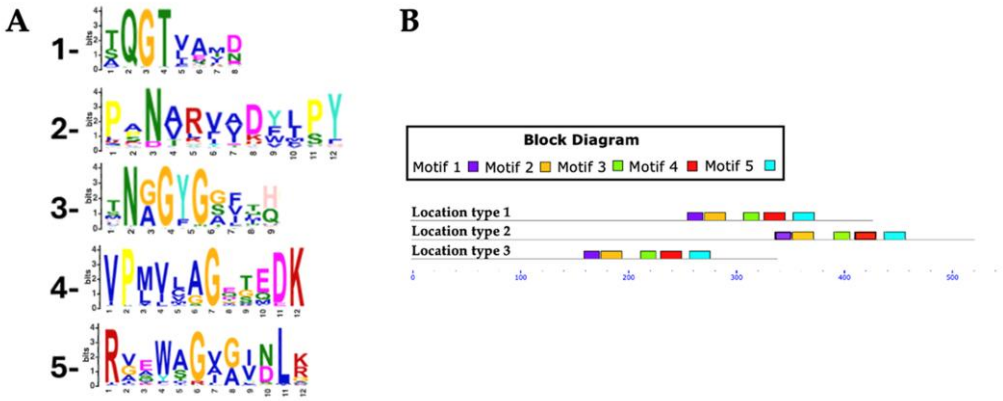

Figure 4. Conserved motifs in Rht2 putative sequences. (A) Sequence logos of conserved motifs. (B) Distribution patterns of motifs in putative Rht2 sequences according to the MAST map.

3.3. Structural Analysis of Predicted RHT Proteins

To explore the structural features of putative RHTs proteins, selected sequences from the conserved motif analysis were used to obtain or model 3D structures in PDB format. When unavailable in the UniProt database, 3D structures were generated using ColabFold v1.5.5: AlphaFold2. Previously reported 3D models of *S. schenckii* Rht1 and Rht2 were used as structural references (Figure 5 and Figure 6) [8].

 doi:10.20944/preprints202505.2096.v1

Figure 5. Three-dimensional structure of Rht1 from *S. schenckii* with predicted motifs highlighted in magenta.

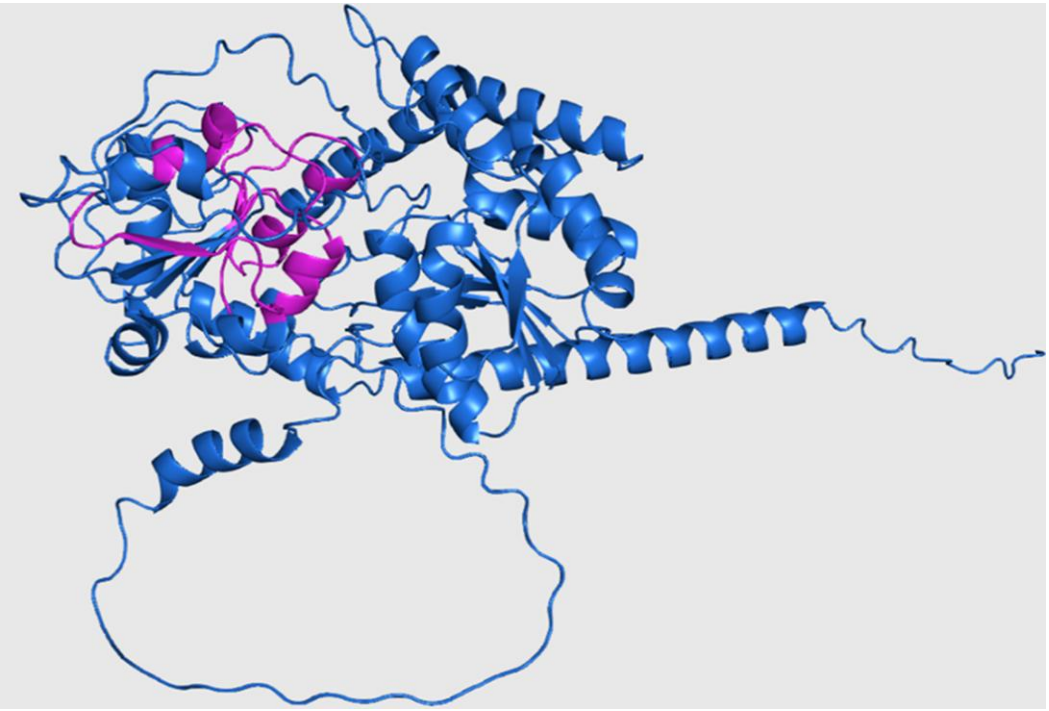

Figure 6. Three-dimensional structure of Rht2 from *S. schenckii* with predicted motifs highlighted in purple.

Rht1 of *S. schenckii* displayed a typical Rossmann-like fold (β/α/β motif), consistent with GT-B glycosyltransferases. Rht2, also from *S. schenckii*, showed two Rossmann folds, reinforcing its classification within the GT-B structural family. Using PyMOL, a total of 23 pairwise alignments were performed for each RHT, including species selected based on HMM results and representing both high and low sequence similarity levels. The RMSD values were used to assess structural similarity, with values <1 considered acceptable [40,41]. These were compared to BLAST-based identity and positive percentages (Tables 2 and 3).

 doi:10.20944/preprints202505.2096.v1

For Rht1, *S. brasiliensis* showed the highest structural similarity (RMSD = 0.14) and 98% positives, consistent with its close phylogenetic relationship to *S. schenckii*. Other species such as *Fonseca erecta* and *Cordyceps militaris* maintained low RMSD values (1.192 & 1.38 respectively) despite having lower positives (54–56%), indicating structural conservation beyond sequence similarity.

For Rht2, a similar trend was observed. For instance, *Colletotrichum graminicola* (48% identity) showed an RMSD of 0.581, suggesting a conserved fold. On the other hand, the organism with the highest RMSD value analyzed was *Lophiotrema nucula*, with a value of 2.101. However, it is important to note that this organism shares only 33% identity with the model Rht2.

Table 2. Structural alignments between Rht1 from *Sporothrix schenckii* and selected fungal species using PyMOL.

Species	Accession number	Residues	RMSD	Identities (%)	Positives (%)
Sporothrix brasiliensis	XP040616120.1	159	0.14	97	98
Ophiostoma piceae	EPE10043.1	162	0.576	64	74
Podospora anserina	XP 001903917.1	129	0.65	40	49
Grosmannia clavigera	XP_014168710	156	0.677	54	66
Ascodesmis nigricans	TGZ82940.1	95	0.678	37	50
Madurella mycetomatis	KXX75366.1	155	0.729	45	56
Thermothelomyces thermophilus	XP_003664509.1	158	0.73	42	54
Podospora comata	VBB80562.1	135	0.75	43	55
Penicillium digitatum	XP_014534696.1	92	0.752	37	52
Thermochaetoides thermophila	XP_006694985.1	144	0.795	38	50
Trichoderma reesei	XP_006961478.1	112	0.795	38	55
Metarhizium guizhouense	KID87172.1	124	0.836	38	52
Aspergillus niger	EHA26758.1	98	0.84	40	54
Paracoccidioides brasiliensis	XP_010757480.1	113	0.872	35	55
Amniculicola lignicola	KAF2003674.1	105	0.964	38	53
Coccidioides immitis	XP_001246780.1	122	0.978	43	55
Thermothielavioides terrestris	SPQ26596.1	156	1.013	41	52
Macrophomina phaseolina	EKG10336.1	119	1.068	35	54
Fonsecaea pedrosoi	XP_013280197.1	123	1.074	36	55
Fonsecaea multimorphosa	XP_016629425.1	127	1.185	36	53
Fonsecaea erecta	XP_018698961.1	126	1.192	35	54
Cordyceps militaris	ATY63072.1	127	1.38	42	56
Friedmanniomyces simplex	TKA63572.1	115	1.468	37	49

Accession Number: Unique identifier assigned to each biological sequence within the NCBI database. **Residues:** The number of residues involved in the three-dimensional structure of the protein from each analyzed species. **RMSD:** The root means square deviation, which measures the average difference between the positions of atoms in two aligned structures, indicating the degree of structural similarity. **Identity (%):** Percentage of exact matches between the amino acid sequences of the aligned proteins. **Positives (%):** Percentage of amino acid residues in the aligned proteins that are similar (though not necessarily identical), calculated based on sequence comparison.

Table 3. Three-dimensional structure alignments between Rht2 from *Sporothrix schenckii* and selected fungal species using PyMOL.

Species	Accession number	Residues	RMSD	Identity (%)	Positives (%)
Colletotrichum graminicola	XP_008100482.1	323	0.581	48	54
Ophiostoma piceae	EPE10437.1	375	0.605	57	65
Calocera cornea	KZT50863.1	345	0.91	39	48
Grosmannia clavigera	XP_014175810.1	252	0.965	26	38
Hyaloscypha hepaticicola	PMD21084.1	263	0.972	35	49
Macrophomina phaseolina	EKG11414.1	263	1.056	26	41

 doi:10.20944/preprints202505.2096.v1

Marssonina coronariae	OWP01936.1	272	1.109	26	41
Madurella mycetomatis	KXX79238.1	268	1.115	24	37
Orbilia oligospora	KAF3191956.1	288	1.131	33	49
Pyrenochaeta sp.	OAL46984.1	237	1.157	22	39
Lasallia pustulata	KAA6413478.1	301	1.16	28	43
Phaeomoniella chlamydospora	KKY20074.1	275	1.222	26	40
Phialocephala subalpina	CZR67232.1	259	1.249	30	47
Podospora anserina	XP_001903477.1	218	1.308	32	48
Arthrobotrys flagrans	RVD83950.1	297	1.316	33	48
Zopfia rhizophila	KAF2191997.1	238	1.361	27	39
Decorospora gaudefroyi	KAF1836052.1	248	1.462	28	41
Thermothielavioides terrestris	XP_003658264.1	280	1.469	25	37
Viridothelium virens	KAF2235942.1	288	1.497	27	39
Dactylellina haptotyla	EPS37979.1	289	1.54	32	48
Mytilinidion resinicola	XP_033568734.1	273	1.551	34	49
Cladophialophora carrionii	XP_008725802.1	275	2.044	26	38
Lophiotrema nucula	KAF2113514.1	257	2.101	33	54

Accession Number: Unique identifier assigned to each biological sequence within the NCBI database. **Residues:** The number of residues involved in the three-dimensional structure of the protein from each analyzed species. **RMSD:** The root means square deviation, which measures the average difference between the positions of atoms in two aligned structures, indicating the degree of structural similarity. **Identity (%):** Percentage of exact matches between the amino acid sequences of the aligned proteins. **Positives (%):** Percentage of amino acid residues in the aligned proteins that are similar (though not necessarily identical), calculated based on sequence comparison.

Simultaneously, the Rht1 and Rht2 proteins were analyzed using the CB-Dock tool to investigate their potential interactions with UDP-L-rhamnose. Figure 7A displays the docking results for Rht1 from *S. schenckii*, revealing high-affinity predictions.

Notably, residues near motif 3, HAGSGSI, exhibited a binding interaction between UDP-L-rhamnose and the amino acid residues V130, R131, and D133. Additionally, residues Y192, Q193, F197, P198, T199, E203, R204, and S205 also showed interactions with the molecule (Figure 7B).

For Rht2 (Figure 8A), the sugar-binding sites included amino acids G321, T322, and I323, corresponding to motif 1 TXGTIA. Additionally, residues N422, G424, Y425, N426, G427, and A430 showed similarity to motif 3 TNAGYNGVXA. Finally, the residues E445, D446, and K447 matched the last four amino acids of motif 4 VPXXXXGXXXDK. Additional interactions with the molecule were observed for residues Y10, A11, G12, H13, N15, P16, I135, P238 F406 and H409 (Figure 8B).

 doi:10.20944/preprints202505.2096.v1

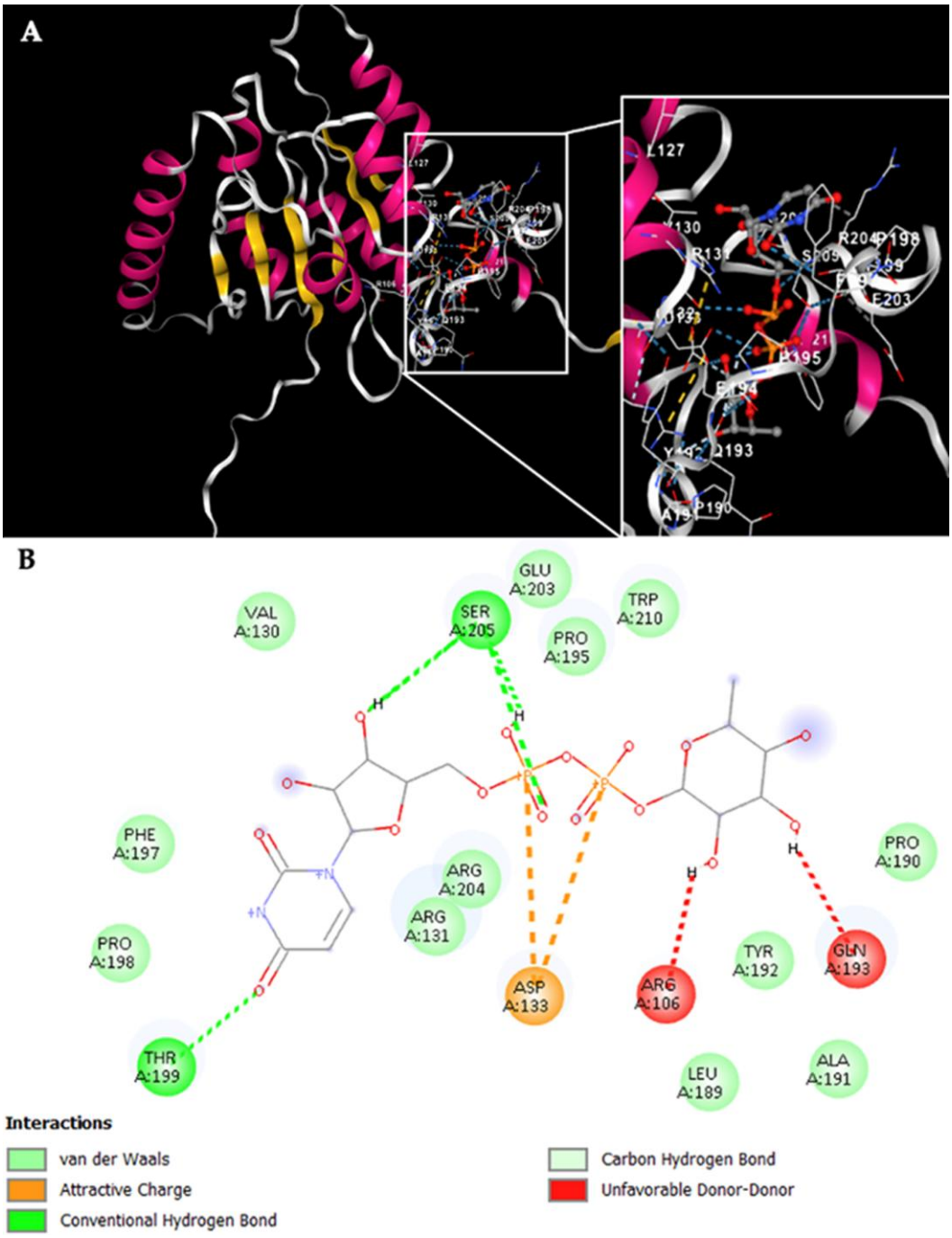

Figure 7. Potential interactions of Rht1 from *S. schenckii* with UDP-L-rhamnose. (**A**) Three-dimensional visualization of the protein–ligand docking complex structure. The white box shows a close-up view of the interaction sites between the protein and the ligand. (**B**) Two-dimensional representation of the same docking complex, showing detailed interactions between the ligand and amino acid residues.

 doi:10.20944/preprints202505.2096.v1

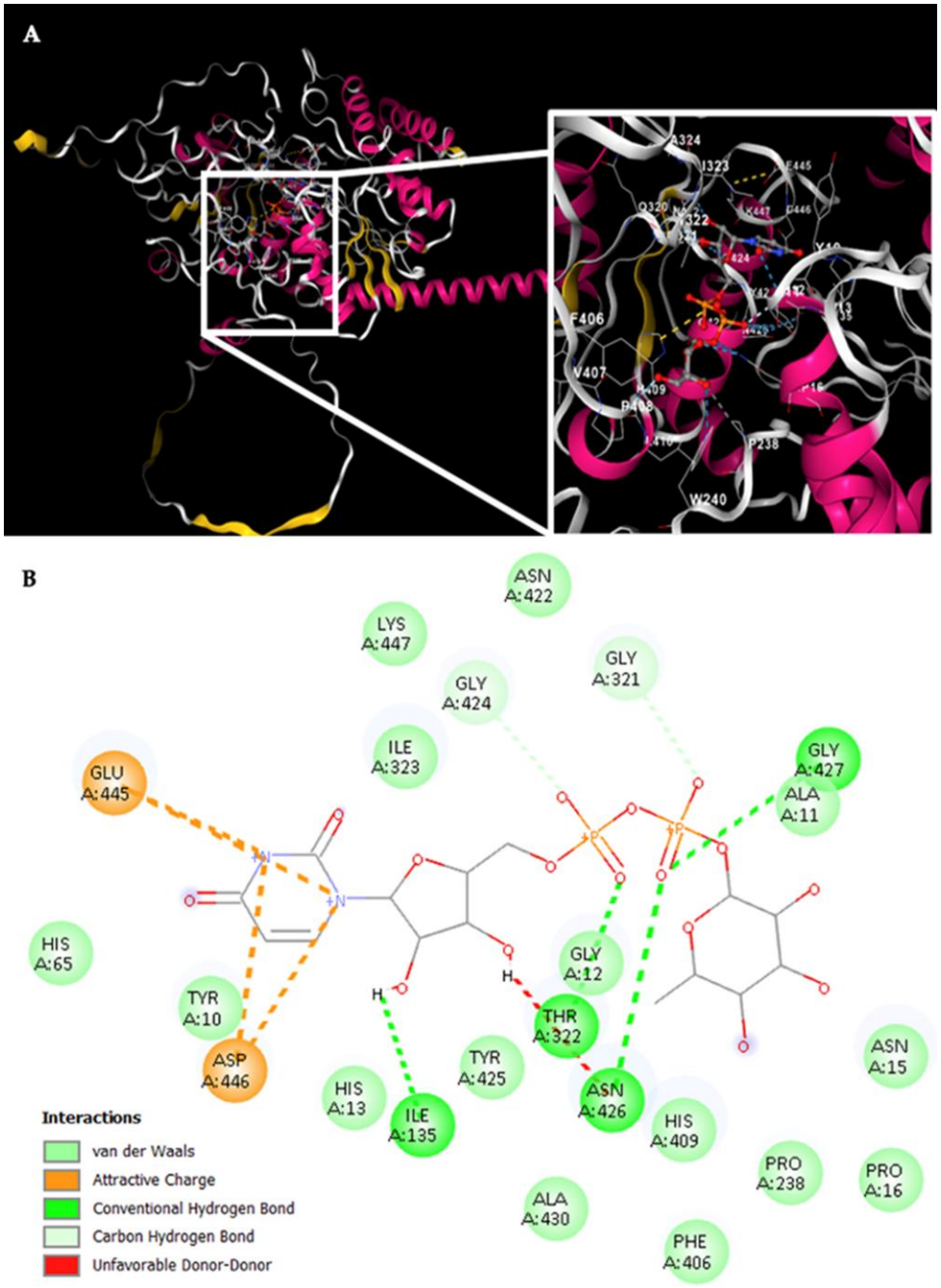

Figure 8. Potential interactions of Rht2 from *S. schenckii* with UDP-L-rhamnose. (**A**) Three-dimensional visualization of the protein–ligand docking complex structure. The white box shows a close-up view of the interaction sites between the protein and the ligand. (**B**) Two-dimensional representation of the same docking complex, showing detailed interactions between the ligand and amino acid residues.

3.4. Molecular Docking Analysis of Putative RHTs

Putative Rht1 and Rht2 proteins identified previously were analyzed using Vina Wizard (PyRx–Python Prescription 0.8) to evaluate their affinity for different sugar donors: UDP-L-rhamnose, UDP-glucose, GDP-mannose, and Dolichol-phosphate-mannose (Dol-P-mannose). This approach aimed to confirm the specificity of rhamnosyltransferases for UDP-L-rhamnose. Binding affinity, expressed as binding free energy (kcal/mol), was used to assess interaction strength—more negative values indicating stronger affinity [31]. For *S. schenckii* Rht1, UDP-L-rhamnose (−7.6 kcal/mol) and GDP-mannose (−7.4 kcal/mol) showed the highest affinities. In contrast, UDP-glucose (−6.0 kcal/mol) and Dol-P-mannose (−6.8 kcal/mol) showed weaker binding. For Rht2, UDP-L-rhamnose (−9.8 kcal/mol) and UDP-mannose (−9.3 kcal/mol) exhibited the strongest affinities, suggesting a substrate preference

 doi:10.20944/preprints202505.2096.v1

for these donors. Given the lower affinities for UDP-glucose and Dol-P-mannose, these substrates were excluded from subsequent analyses to focus on those with higher biological relevance.

Tables 4 and 5 show the molecular docking results for putative Rht1 and Rht2 proteins across various fungal species. In general, most species exhibited a higher binding affinity for UDP-L-rhamnose compared to GDP-mannose, suggesting a preferential interaction with this sugar donor. For instance, *T. reesei* showed a strong preference for UDP-L-rhamnose (−8.9 kcal/mol) over GDP-mannose (−7.9 kcal/mol) in the Rht1 analysis. A similar trend was observed among the putative Rht2 proteins, where *M. anisopliae* showed the highest affinity for UDP-L-rhamnose (−9.7 kcal/mol) relative to GDP-mannose (−8.7 kcal/mol). Likewise, *M. guizhouense* and *T. harzianum* exhibited greater affinities for UDP-L-rhamnose (−9.3 and −9.5 kcal/mol, respectively) than for GDP-mannose (−9.0 and −8.8 kcal/mol, respectively).

Table 4. Molecular docking analysis between species with putative Rht1 proteins.

Species	Accession number	Binding affinity (Kcal/mol)	
		UDP-L-rhamnose	GDP-Mannose
Sporothrix schenckii	XP_016583713.1	-7.6	-7.4
Aspergillus niger	EHA26758.1	-7.7	-7.6
Metarhizium anisopliae	KJK84664.1	-7.1	-7.1
Metarhizium guizhouense	KID87172.1	-8.3	-7.4
Trichoderma atroviride	XP_013943227.1	-7.3	-7.2
Trichoderma reesei	XP_006961478.1	-8.9	-7.9
Trichoderma virens	XP_013961374.1	-7.5	-7.2

Accession Number: Unique identifier assigned to each biological sequence within the NCBI database. The columns "UDP-L-Rhamnose" and "GDP-Mannose" show the binding affinities between each protein and these specific ligands, expressed in kilocalories per mole (kcal/mol).

Table 5. Molecular docking analysis between species with putative Rht2 proteins.

Species	Accession number	Binding affinity (Kcal/mol)	
		UDP-L-rhamnose	GDP-Mannose
Sporothrix schenckii	XP_016584143.1	-9.8	-9.3
Aspergillus niger	GKZ64237.1	-7.7	-7.6
Metarhizium anisopliae	KJK80520.1	-9.7	-8.7
Metarhizium guizhouense	KID92007.1	-9.3	-9
Trichoderma atroviride	UKZ67550.1	-7.3	-7.1
Trichoderma harzianum	KKO97596.1	-9.5	-8.8
Trichoderma reesei	XP_006968899.1	-8.8	-8.3
Trichoderma virens	XP_013957984.1	-8.3	-7.4

Accession Number: Unique identifier assigned to each biological sequence within the NCBI database. The columns "UDP-L-Rhamnose" and "GDP-Mannose" show the binding affinities between each protein and these specific ligands, expressed in kilocalories per mole (kcal/mol).

3.5. In Silico Site-Directed Mutagenesis

Site-directed mutagenesis analyses were performed using the CHARMM-GUI platform [35] to assess the impact of specific amino acid substitutions on the binding affinity of predicted RHTs toward UDP-L-rhamnose.

Initial docking controls with *S. schenckii* Rht1 showed the highest affinity for UDP-L-rhamnose (−8.7 kcal/mol), compared to UDP-glucose (−8.5 kcal/mol) and GDP-mannose (−8.3 kcal/mol), confirming substrate specificity.

Subsequent in silico substitutions in Rht1 identified Y192 as critical for substrate interaction. Its replacement with serine (Y192S) led to a notable reduction in affinity, especially for UDP-L-rhamnose (−8.3 kcal/mol), indicating a change of 0.5 kcal/mol.

 doi:10.20944/preprints202505.2096.v1

This approach was extended to other putative Rht1 proteins. In *Beauveria bassiana*, mutation W115A reduced affinity from −9.1 to −7.9 kcal/mol, while W114A in *Fusarium oxysporum* caused a change of 1.1 kcal/mol (from −8.9 to −7.8 kcal/mol), reducing affinity. Conversely, *Madurella mycetomatis* with mutation W208A showed a minimal change (−8.2 to −8.1 kcal/mol), suggesting a limited role for this residue. In *Fonsecaea pedrosoi*, L121S decreased binding affinity by 0.9 kcal/mol (from −8.6 to −7.7 kcal/mol), potentially indicating a stabilizing role in ligand interaction.

Docking controls for the Rht2 protein revealed the highest binding affinity for UDP-L-rhamnose (−9.3 kcal/mol), followed by GDP-mannose (−8.9 kcal/mol) and UDP-glucose (−8.2 kcal/mol). Substitution mutations were performed, and the most significant effects were observed with the double mutation H13S/D446A in *S. schenckii*, which reduced the binding affinity to UDP-L-rhamnose to −8.0 kcal/mol, representing a change of 1.3 kcal/mol. A moderate reduction was also observed for GDP-mannose (−8.4 kcal/mol, change of 0.5 kcal/mol), while affinity for UDP-glucose increased to −8.9 kcal/mol (change of 0.7 kcal/mol).

Among all evaluated species, *S. schenckii* exhibited the greatest reduction in ligand binding mutation, suggesting that H13 and D446 play critical roles in substrate interaction. Additionally, *Ophiostoma piceae* and *Xylona heveae* showed the highest wild-type affinities (−10.0 kcal/mol), with changes of 0.8 and 0.7 kcal/mol, respectively, upon mutation. In contrast, *T. reesei* lacked an orthologous residue at the position corresponding to H13 in *S. schenckii*, so alternative residues involved in UDP-L-rhamnose binding were targeted. Mutants H302S and P221A showed minimal changes in affinity, with only a 0.1 kcal/mol change (from −8.9 to −8.8 kcal/mol), suggesting these residues are not key to substrate interaction.

In *Macrophomina phaseolina*, the H19S/D378A mutation resulted in a 0.5 kcal/mol reduction in binding affinity (from −9.5 to −9.0 kcal/mol), while in *Magnaporthiopsis poae* (H31S/D383A) the decrease was smaller (0.2 kcal/mol), indicating greater tolerance to substitutions at these positions.

These findings highlight the importance of specific residues in maintaining the stability of protein-ligand interactions and provide valuable insights for future structure-function optimization of these enzymes. Structural similarity between wild-type and mutant proteins was assessed using RMSD values to confirm that the observed affinity changes were attributable to residue substitution rather than major conformational alterations. Results are detailed in Tables 6 and 7.

Table 6. In silico site-directed mutagenesis of putative Rht1 proteins.

Species	Mutated Residue	Binding Affinity (Kcal/mol)		RMSD
		WT	PM	
Sporothrix schenckii	Y192S	-8.7	-8.3	0.00 (232 a.a)
Aspergillus niger	L122A	-7.5	-7.3	0.00 (159 a.a)
Metarhizium brunneum	W116A	-9.0	-8.5	0.00 (211 a.a)
Trichoderma reesei	W112A	-8.6	-8.0	0.00 (201 a.a)
Trichoderma atroviride	W112A	-8.3	-7.9	0.00 (207 a.a)
Trichoderma virens	W112A	-8.3	-7.8	0.00 (207 a.a)
Madurella mycetomatis	W208A	-8.2	-8.1	0.00 (331 a.a)
Fonsecaea pedrosoi	L121S	-8.6	-7.7	0.00 (205 a.a)
Neonectria ditissima	W114A	-8.9	-8.4	0.00 (208 a.a)
Beauveria bassiana	W115A	-9.1	-7.9	0.00 (209 a.a)
Fusarium oxysporum	W114A	-8.9	-7.8	0.00 (208 a.a)

A.A. MUT: Mutated amino acids; **WT:** Wild-type protein; **PM:** Mutated protein; **RMSD:** Alignment between the wild-type and the mutated protein.

 doi:10.20944/preprints202505.2096.v1

Table 7. In silico site-directed mutagenesis of putative Rht2 proteins.

Species	Mutated Residue	Binding Affinity (Kcal/mol)		RMSD
		WT	PM	
Sporothrix schenckii	H13S, D446A	-9.3	-8.0	0.00 (576 a.a)
Ophiostoma piceae	G135S, D563A	-10.0	-9.2	0.00 (695 a.a)
Xylona heveae	H15S, D386A	-10.0	-9.3	0.00 (461 a.a)
Magnaporthiopsis poae	H31S, D383A	-9.5	-9.3	0.00 (461 a.a)
Botrytis cinerea	H19S, E379A	-8.7	-8.2	0.00 (452 a.a)
Macrophomina phaseolina	H19S, D378A	-9.5	-9.0	0.00 (449 a.a)
Aspergillus niger	H29E, T298F	-9.6	-9.3	0.00 (456 a.a)
Madurella mycetomatis	L250S	-9.4	-9.2	0.00 (452 a.a)
Metarhizium brunneum	P34G, M242G	-9.5	-9.2	0.00 (457 a.a)
Trichoderma ressei	H302S, P221A	-8.9	-8.8	0.00 (418 a.a)

A.A. MUT: Mutated amino acids; **WT:** Wild-type protein; **PM:** Mutated protein; **RMSD:** Alignment between the wild-type and the mutated protein.

3.6. Cell Wall Carbohydrate Composition in Species with Putative RHTs

To assess the presence of rhamnose in some species with putative Rht1 and Rht2 proteins, the carbohydrate composition of the cell wall was analyzed. Quantified carbohydrates included rhamnose, glucosamine, glucose, mannose, and galactose. Values were normalized to represent relative percentages, adding to 100%.

Glucose was the predominant sugar, ranging from 47.91% to 76.33%, with *M. guizhouense* showing the highest content. Mannose exhibited high variability (0.46% to 19.3%), being most abundant in *M. brunneum*. Notably, rhamnose—a sugar previously unreported in most of these organisms—was detected in all analyzed species, reaching up to 4.07% in *T. virens*. Full results are presented in Figure 9.

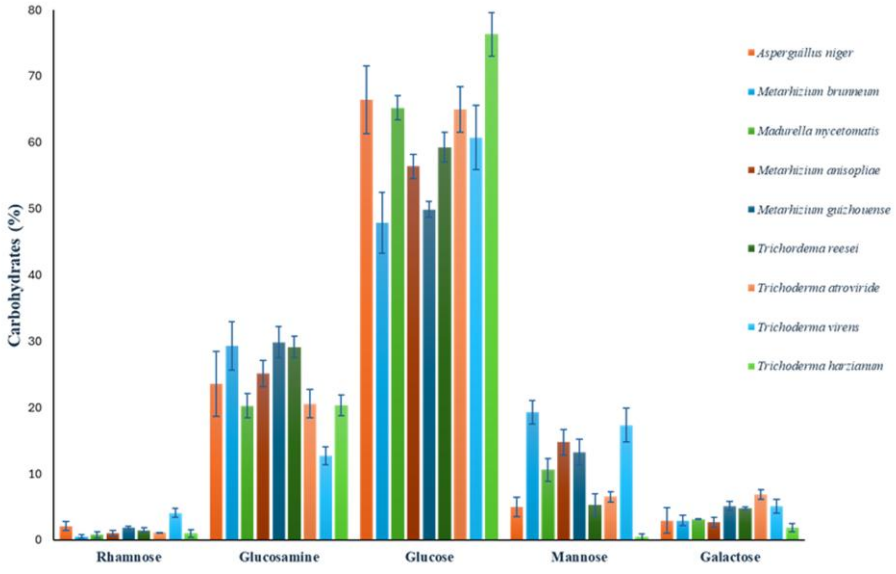

Figure 9. Cell wall carbohydrate composition in species with putative RHTs. Error bars represent the mean ± SD from three biological replicates per condition.

3.7. Enzymatic Analysis of Putative RHTs

To determine whether the predicted species exhibited any RHT activity, we measured enzyme activity in cell homogenates, with α-1,6-mannobiose as the rhamnose acceptor and UDP-L-rhamnose

 doi:10.20944/preprints202505.2096.v1

as the donor. Reaction products were analyzed by HPAEC-PAD, and results were expressed as trisaccharide min^{-1} per mg $protein^{-1}$.

The highest enzymatic activity was observed in *S. schenckii* (123.63 ± 18.46 trisaccharide min^{-1} mg $protein^{-1}$), consistent with prior knowledge of its ability to utilize UDP-L-rhamnose. In contrast, negative controls *Candida albicans* and *Saccharomyces cerevisiae* exhibited near-zero activity, confirming the absence of RHT activity in these species. Intermediate activity levels were detected in *Aspergillus niger* (59.47 ± 3.91 trisaccharide min^{-1} mg $protein^{-1}$), *Trichoderma virens* (68.03 ± 10.31 trisaccharide min^{-1} mg $protein^{-1}$), and *Trichoderma reesei* (39.20 ± 7.15 trisaccharide min^{-1} mg $protein^{-1}$), suggesting rhamnose transfer function in these organisms. Low activity observed in the no acceptor condition supports the enzymatic specificity, and residual values with inactivated protein confirm the association with RHT processes. Enzymatic analysis results are summarized in Table 8.

Table 8. Enzymatic analysis of putative RHTs.

Species	UDP-Rhamnose	Without acceptor	UDP-L-Rhamnose and inactivated protein
Sporothrix schenckii	123.63 ± 18.46	1.40 ± 0.53	0.08 ± 0.03
Candida albicans	0.12 ± 0.08	0.17 ± 0.06	0.02 ± 0.03
Saccharomyces cerevisiae	0.17 ± 0.12	0.05 ± 0.05	0.02 ± 0.03
Aspergillus niger	59.47 ± 3.91	0.87 ± 0.25	0.15 ± 0.09
Madurella mycetomatis	37.47 ± 6.14	0.93 ± 0.42	0.10 ± 0.00
Metarhizium anisopliae	35.77 ± 7.07	1.27 ± 0.35	0.13 ± 0.12
Metarhizium brunneum	28.40 ± 7.37	1.37 ± 0.61	0.17 ± 0.06
Metarhizium guizhouense	29.23 ± 6.65	0.40 ± 0.20	0.12 ± 0.08
Trichoderma atroviride	30.93 ± 6.81	0.80 ± 0.35	0.07 ± 0.06
Trichoderma harzianum	31.70 ± 7.88	0.63 ± 0.31	0.07 ± 0.12
Trichoderma reesei	39.20 ±7.15	0.63 ± 0.23	0.08 ± 0.10
Trichoderma virens	68.03 ± 10.31	1.10 ± 0.44	0.10 ± 0.10

Expressed as trisaccharide min^{-1} per mg $protein^{-1}$. Results express the mean ± SD, n=3.

4. Discussion

Using HMM profiles, we identified putative Rht1 and Rht2 sequences from the fungal portion of the NCBI NR database. This approach is effective for detecting distant orthologs, though its success depends on the completeness and annotation quality of genomic data [42]. The limited representation of certain fungal groups likely reflects the under-sequencing of these taxa.

Our results revealed a broad taxonomic distribution of RHTs, especially in ecologically and biotechnologically relevant fungi. Rht1 was most frequent in *Aspergillus*, *Penicillium*, and *Fusarium*, while Rht2 predominated in *Fusarium* and *Colletotrichum*. These genera are known for pathogenesis and secondary metabolite production, with some species acting as plant pathogens and others as producers of industrial enzymes or mycotoxins [43–52].

The co-occurrence of Rht1 and Rht2 in 126 genera suggests complementary metabolic functions. Notably, both RHTs were found in endophytic and saprophytic fungi like *Trichoderma*, *Claviceps*, and *Xylaria*, indicating roles beyond pathogenesis [53–57].

From an evolutionary perspective, the presence of Rht1 and Rht2 in diverse taxonomic lineages suggests a functional distribution of these enzymes within the fungal kingdom, particularly in the phylum *Ascomycota*. However, they appear to be absent in other phyla, such as *Basidiomycota*. Previous studies analyzing members of *Basidiomycota* have shown that their cell walls are primarily composed of glucose, mannose, and galactose, with occasional presence of xylose and fucose, but a consistently low or absent content of rhamnose, suggesting ecological and functional differences [58]. These compositional differences likely reflect distinct ecological strategies: Basidiomycetes are specialized in lignocellulose degradation [59], whereas Ascomycetes, which often colonize rhamnose-

 doi:10.20944/preprints202505.2096.v1

rich plant tissues, may be associated with their direct interactions with plant hosts in survival, saprophytic, mutualistic, or pathogenic contexts [52,60–63].

The evolutionary origin of RHTs may involve vertical inheritance, horizontal gene transfer, or gene loss in certain lineages. Alternatively, these enzymes may have originated within the fungal kingdom, with Basidiomycota either losing or never utilizing rhamnose and RHTs, instead adapting their cell wall and glycoconjugate structures to other substrates typical of their environment [64].

To explore the evolutionary history and diversification of RHTs, we compared the phylogenetic and taxonomic relationships among fungi with putative Rht1 and Rht2. In the case of Rht1, the clustering of taxonomically distant genera, such as *Pyricularia* and *Sporothrix, despite their ecological differences, suggests potential structural or functional conservation of RHTs, possibly related to polysaccharide biosynthesis or host*/environmental adaptation [8,65]. Similarly, the grouping of phytopathogens like *Magnaporthiopsis* and *Monosporascus* may reflect convergent evolution driven by plant-associated lifestyles [66,67]. For Rht2, phylogenetic and taxonomic trees reveal a notable congruence in the clustering of fungal genera. Genera ranging from phytopathogens and entomopathogens to biocontrol agents highlight a potentially broad adaptive role for Rht2, possibly involving the regulation of cell wall architecture and participation in host or environmental interaction mechanisms. For instance, enzymatic activities associated with host invasion or decomposition, such as rhamnose-dependent pectin degradation in *Colletotrichum* [68], and substrate colonization traits in *Trichoderma* and *Purpureocillium*, may reflect conserved Rht2 functions supporting ecological adaptation [52,54]. In addition to these cases, other genera distributed across diverse taxonomic orders were also identified, suggesting possible retention or functional convergence of RHTs across Ascomycota lineages [69–73].

These findings provide valuable insight into the evolutionary relationships among RHT-containing fungi and support the hypothesis that these enzymes share conserved sequence motifs, alongside taxon-specific variations associated with functional diversification within the fungal kingdom. The high degree of conservation observed in motifs such as TXGATXXF, LXXQXG, and HAGXGXI, in Rht1, and XQGT and XNXGYG in Rht2, suggests that these sequence elements are critical for the catalytic activity and/or substrate recognition. Despite minor variation in motif starting positions among RHTs sequences, the spacing between conserved motifs remained consistent. This variation in initial motif positions may suggest differences in the N-terminal regions of these proteins, potentially due to divergence in sequence length or domain architecture across species. Such conservation in inter-motif distances may reflect evolutionary constraints that maintain the integrity of the active site and support a conserved enzymatic function across species. The absence of motif 5 (Rht1) in a larger number of sequences could indicate functional divergence or a loss of secondary features that are not essential for the primary enzymatic activity. This suggests that the catalytic region is structurally preserved across sequences, reinforcing the idea of a conserved functional domain even amid sequence diversity. Notably, these motifs showed no similarity to previously characterized canonical glycosyltransferases. While GT-A-type glycosyltransferases typically exhibit the conserved Asp-X-Asp (DXD) motif implicated in divalent cation coordination and nucleotide-sugar stabilization, this feature was not observed in the RHTs sequences examined. Although conserved motifs like DXD are common in glycosyltransferases, they are not universal nor strictly indicative of function, as motif structure and context can vary widely among families, reflecting their functional and structural diversity [74–76].

The analysis of Rht1 and Rht2 sequences reveals substantial conservation among phylogenetically related species, suggesting functional preservation across divergent lineages. In the case of Rht1, structural alignments with more distantly related species, such as *Fusarium erecta* and *Cordyceps militaris*, showed moderate sequence identities (54-56%) but retained low RMSD scores. Similarly, for Rht2, the alignment between *C. graminicola* and *S. schenckii* yielded an RMSD of 0.581 despite low sequence identity. These results suggest that essential structural elements, particularly those involved in substrate binding or catalytic site stabilization, may be conserved even when amino acid sequences differ significantly [75–77]. Collectively, these findings are in line with previous

 doi:10.20944/preprints202505.2096.v1

reports emphasizing the evolutionary plasticity of glycosyltransferase sequences alongside the conservation of structurally and functionally critical domains [76]. The observed structural conservation among both closely related and taxonomically distant fungal species suggests that RHTs may have undergone evolutionary adaptation to diverse ecological niches while retaining their essential biological roles.

To assess the functional relevance of the observed structural similarities, molecular docking analysis was performed between the putative RHTs and UDP-L-rhamnose. In *S. schenckii*, both Rht1 and Rht2 exhibited the highest affinity for UDP-L-rhamnose, consistent with previous studies reporting enzymatic interaction with this substrate [8]. In contrast, GDP-mannose, UDP-glucose, and Dol-P-mannose showed lower binding affinities, suggesting fewer stable interactions and limited functional relevance. Most putative Rht1 and Rht2 proteins exhibited a consistent preference for UDP-L-rhamnose over GDP-mannose, indicating the specificity of these RHTs for UDP-L-rhamnose as a substrate. Moreover, the co-localization of predicted motifs with substrate-binding sites supports the potential role of these proteins as functional RHTs.

In silico site-directed mutagenesis was conducted to explore structural determinants of substrate specificity in putative RHTs. Targeted amino acid substitutions in Rht1, such as Y192S in *S. schenckii* and W115A in *B. bassiana*, led to measurable reductions in binding affinity to UDP-L-rhamnose, highlighting the functional importance of these residues. In Rht2, mutations H13S and D446A induced an even greater loss of affinity, suggesting that these residues are particularly critical for substrate stabilization.

Interestingly, the affected residues in fungal RHTs correspond to key catalytic residues previously identified in plant RHTs. For example, H22 and D121 in UGT71G1 (*Medicago truncatula*), H20 and D119 in VvGT1 (*Vitis vinifera*), and H21 and S124 in UGT89C1 (*A. thaliana*) are known to be part of the catalytic site that directly interacts with the UDP -L-rhamnose [78,79]. Similarly, in MrUGT78R1 from *Morella rubra*, mutations at D406 completely abolished RHT activity [80].

The parallels between the plant and fungal enzymes suggest that the catalytic core of RHTs is evolutionarily conserved, with histidine and aspartate residues playing central roles in substrate coordination and catalysis. Supporting this, cell wall composition analysis confirmed the presence of rhamnose in the studied fungal species, despite its prior unreported detection in most of them.

Glucose was identified as the main component of the fungal cell wall, consistent with its well-established structural role in fungi [81]. Mannose content showed high variability among species (0.46%–19.3%), with the highest levels observed in *M. brunneum*. Mannose is typically associated with glycoproteins and mannans involved in cell adhesion and environmental interactions [82].

Rhamnose was detected in all species analyzed. The presence of this sugar in the cell walls of fungal species identified as potential RHTs carriers supports the proposition that these enzymes may be actively involved in rhamnosylation processes. However, this finding also raises new questions regarding the specific role of rhamnose in the structure and dynamics of the fungal cell wall, as well as the identity of the polysaccharides in which it may be incorporated. Beyond the species analyzed in this study, rhamnose has also been reported in other fungal genera, such as *Rhynchosporium secalis*, *Penicillium chrysogenum*, and in the spore mucilage of *C. graminicola*, which contains glycoproteins with rhamnose [52,83,84]. Additionally, functional genes involved in UDP-L-rhamnose biosynthesis, such as UG4,6-Dh and U4k6dG-ER, have been identified in *Magnaporthe grisea* and *B. cinerea* [85].

These findings support the idea that rhamnosylation is a conserved process in fungal lineages, potentially mediated by the putative RHTs identified in this study. Differences in other sugar components further highlight species-specific variations in cell wall architecture and functionality.

The detection of rhamnose in the cell walls of all analyzed species, along with the observed rhamnose transfer activity using UDP-L-rhamnose as donor and α-1,6-mannobiose as acceptor, provides functional evidence for the role of these enzymes. Notably, *S. schenckii* exhibited the highest transfer rate, consistent with previously reported use of UDP-L-rhamnose [8], while other species such as *A. niger*, *T. virens*, and *T. reesei* showed intermediate RHT activity levels, suggesting the presence of functional RHTs with varying degrees of activity.

 doi:10.20944/preprints202505.2096.v1

In contrast, the absence of RHT activity in *C. albicans* and *S. cerevisiae*, both of which lack rhamnose in their cell walls [86], reinforces the specificity of the enzymatic process and suggests that rhamnose incorporation is restricted to certain fungal lineages. Together, cell wall composition and enzymatic activity analyses support a model in which rhamnose incorporation into the fungal cell wall is mediated by RHTs. The variability in activity levels suggests potential differences in enzyme regulation or precursor availability across species.

5. Conclusions

This study highlights the evolutionary and functional relevance of RHTs in fungi by integrating computational, phylogenetic, structural, and biochemical approaches. The application of HMM enabled the sensitive detection of putative RHTs across diverse fungal taxa, revealing a heterogeneous but phylogenetically enriched distribution, particularly in Ascomycota, which suggests an evolutionary trajectory of functional specialization. Conserved sequence motifs identified in putative RHTs, and their proximity to residues predicted to interact with the UDP-L-rhamnose substrate in molecular docking analyses, support the existence of lineage-specific functional adaptations. These findings support a model in which rhamnose incorporation into the fungal cell wall is a conserved but restricted process, mediated by specialized RHTs in fungal lineages.

Supplementary Materials: The following supporting information can be downloaded at the website of this paper posted on Preprints.org.

Funding: This work was supported by the Secretaría de Ciencia, Humanidades, Tecnología e Innovación [Ciencia de Frontera 2019-6380 and CBF2023-2024-655], and Red Temática Glicociencia en Salud [CONACYT-México].

References

1. Stajich, J.E.; Berbee, M.L.; Blackwell, M.; Hibbett, D.S.; James, T.Y.; Spatafora, J.W.; Taylor, J.W. The Fungi. *Curr. Biol.* **2009**, 19.
2. Choi, J.J.; Kim, S.H. A Genome Tree of Life for the Fungi Kingdom. *Proc. Natl. Acad. Sci. U S A* **2017**, 114, 9391–9396, doi:10.1073/pnas.1711939114.
3. Naranjo-Ortiz, M.A.; Gabaldón, T. Fungal Evolution: Diversity, Taxonomy and Phylogeny of the Fungi. *Biol. Rev.* **2019**, 94, 2101–2137, doi:10.1111/brv.12550.
4. Stajich, J.E. Fungal Genomes and Insights into the Evolution of the Kingdom. *Microbiol. Spectr.* **2017**, 5, doi:10.1128/microbiolspec.funk-0055-2016.
5. Ruiz-Herrera, J.; Ortiz-Castellanos, L. Analysis of the Phylogenetic Relationships and Evolution of the Cell Walls from Yeasts and Fungi. *FEMS Yeast Res.* **2010**, 10, 225–243.
6. Gonçalves, D. de S.; Rodriguez de La Noval, C.; Ferreira, M. da S.; Honorato, L.; Araújo, G.R. de S.; Frases, S.; Pizzini, C.V.; Nosanchuk, J.D.; Cordero, R.J.B.; Rodrigues, M.L.; et al. *Histoplasma capsulatum* Glycans from Distinct Genotypes Share Structural and Serological Similarities to *Cryptococcus neoformans* Glucuronoxylo-mannan. *Front. Cell Infect. Microbiol.* **2021**, 10, doi:10.3389/fcimb.2020.565571.
7. Lozoya-Pérez, N.E.; Casas-Flores, S.; de Almeida, J.R.F.; Martínez-Álvarez, J.A.; López-Ramírez, L.A.; Jannuzzi, G.P.; Trujillo-Esquivel, E.; Estrada-Mata, E.; Almeida, S.R.; Franco, B.; et al. Silencing of OCH1 Unveils the Role of *Sporothrix schenckii* N-Linked Glycans during the Host–Fungus Interaction. *Infect. Drug Resist.* **2019**, 12, 67–85, doi:10.2147/IDR.S185037.
8. Mora-Montes, H.M.; García-Gutiérrez, K.; García-Carnero, L.C.; Lozoya-Pérez, N.E.; Ramirez-Prado, J.H. The Search for Cryptic L-Rhamnosyltransferases on the *Sporothrix schenckii* Genome. *J. Fungi* **2022**, 8, doi:10.3390/jof8050529.
9. Yang, Y.; Liang, Y.; Cui, F.; Wang, Y.; Sun, L.; Zan, X.; Sun, W. UDP-Glycosyltransferases in Edible Fungi: Function, Structure, and Catalytic Mechanism. *Ferment.* **2023**, 9.

 doi:10.20944/preprints202505.2096.v1

10. Kikuchi, N.; Kwon, Y.D.; Gotoh, M.; Narimatsu, H. Comparison of Glycosyltransferase Families Using the Profile Hidden Markov Model. *Biochem. Biophys. Res. Commun.* **2003**, 310, 574–579, doi:10.1016/j.bbrc.2003.09.031.
11. Drula, E.; Garron, M.L.; Dogan, S.; Lombard, V.; Henrissat, B.; Terrapon, N. The Carbohydrate-Active Enzyme Database: Functions and Literature. *Nucleic. Acids. Res.* **2022**, 50, D571–D577, doi:10.1093/nar/gkab1045.
12. Yonekura-Sakakibara, K.; Hanada, K. An Evolutionary View of Functional Diversity in Family 1 Glycosyltransferases. *Plant J.* **2011**, 66, 182–193, doi:10.1111/j.1365-313X.2011.04493.x.
13. Wagstaff, B.A.; Zorzoli, A.; Dorfmueller, H.C. Ndp-Rhamnose Biosynthesis and Rhamnosyltransferases: Building Diverse Glycoconjugates in Nature. *Biochem. J.* **2021**, 478, 685–701.
14. Lopes-Bezerra, L.M. *Sporothrix schenckii* Cell Wall Peptidorhamnomannans. *Front. Microbiol.* **2011**, 2.
15. Rollin-Pinheiro, R.; Xisto, M.I.D. da S.; Rochetti, V.P.; Barreto-Bergter, E. *Scedosporium* Cell Wall: From Carbohydrate-Containing Structures to Host–Pathogen Interactions. *Mycopathol.* **2020**, 185, 931–946.
16. Albuquerque, P.C.; Cordero, R.J.B.; Fonseca, F.L.; Peres da Silva, R.; Ramos, C.L.; Miranda, K.R.; Casadevall, A.; Puccia, R.; Nosanchuk, J.D.; Nimrichter, L.; et al. A *Paracoccidioides brasiliensis* Glycan Shares Serologic and Functional Properties with Cryptococcal Glucuronoxylomannan. *Fungal Genet. Biol.* **2012**, 49, 943–954, doi:10.1016/j.fgb.2012.09.002.
17. Wilson, A.E.; Tian, L. Phylogenomic Analysis of UDP-Dependent Glycosyltransferases Provides Insights into the Evolutionary Landscape of Glycosylation in Plant Metabolism. *Plant J.* **2019**, 100, 1273–1288, doi:10.1111/tpj.14514.
18. Takenaka, Y.; Kato, K.; Ogawa-Ohnishi, M.; Tsuruhama, K.; Kajiura, H.; Yagyu, K.; Takeda, A.; Takeda, Y.; Kunieda, T.; Hara-Nishimura, I.; et al. Pectin RG-I Rhamnosyltransferases Represent a Novel Plant-Specific Glycosyltransferase Family. *Nat. Plant.* **2018**, 4, 669–676.
19. Sayers, E.W.; Bolton, E.E.; Brister, J.R.; Canese, K.; Chan, J.; Comeau, D.C.; Connor, R.; Funk, K.; Kelly, C.; Kim, S.; et al. Database Resources of the National Center for Biotechnology Information. *Nucleic. Acids Res.* **2022**, 50, D20–D26, doi:10.1093/nar/gkab1112.
20. Mistry, J.; Chuguransky, S.; Williams, L.; Qureshi, M.; Salazar, G.A.; Sonnhammer, E.L.L.; Tosatto, S.C.E.; Paladin, L.; Raj, S.; Richardson, L.J.; et al. Pfam: The Protein Families Database in 2021. *Nucleic. Acids Res.* **2021**, 49, D412–D419, doi:10.1093/nar/gkaa913.
21. Mirdita, M.; Schütze, K.; Moriwaki, Y.; Heo, L.; Ovchinnikov, S.; Steinegger, M. ColabFold: Making Protein Folding Accessible to All. *Nat. Methods* **2022**, 19, 679–682, doi:10.1038/s41592-022-01488-1.
22. Camacho, C.; Coulouris, G.; Avagyan, V.; Ma, N.; Papadopoulos, J.; Bealer, K.; Madden, T.L. BLAST+: Architecture and Applications. *BMC Bioinform* **2009**, 10, 1–9, doi:10.1186/1471-2105-10-421/FIGURES/4.
23. Katoh, K.; Rozewicki, J.; Yamada, K.D. MAFFT Online Service: Multiple Sequence Alignment, Interactive Sequence Choice and Visualization. *Brief. Bioinform.* **2018**, 20, 1160–1166, doi:10.1093/bib/bbx108.
24. Eddy, S.R. Accelerated Profile HMM Searches. *PLoS Comput Biol* **2011**, *7*, e1002195, doi:10.1371/JOURNAL.PCBI.1002195.
25. Choudhuri, S. Sequence Alignment and Similarity Searching in Genomic Databases: BLAST and FASTA. In Bioinformatics for Beginners. *Acad. Press* **2014**; pp. 133–155.
26. Bailey, T.L.; Johnson, J.; Grant, C.E.; Noble, W.S. The MEME Suite. *Nucleic. Acids Res.* **2015**, 43, 39–49, doi:10.1093/nar/gkv416.
27. Guindon, S.; Dufayard, J.-F.; Lefort, V.; Anisimova, M.; Hordijk, W.; Gascuel, O.; Pour, A. New Algorithms and Methods to Estimate Maximum-Likelihood Phylogenies: Assessing the Performance of PhyML 3.0. *Syst. Biol.* **2010**, 59, 307–321.
28. Bateman, A.; Martin, M.J.; Orchard, S.; Magrane, M.; Ahmad, S.; Alpi, E.; Bowler-Barnett, E.H.; Britto, R.; Bye-A-Jee, H.; Cukura, A.; et al. UniProt: The Universal Protein Knowledgebase in 2023. *Nucleic. Acids. Res.* **2023**, *51*, D523–D531, doi:10.1093/nar/gkac1052.
29. Schrödinger, L.L.C.; DeLano, W. The PyMOL Molecular Graphics System, Version 3.0.
30. Liu, Y.; Grimm, M.; Dai, W. tao; Hou, M. chun; Xiao, Z.X.; Cao, Y. CB-Dock: A Web Server for Cavity Detection-Guided Protein–Ligand Blind Docking. *Act. Pharmacol. Sin.* **2020**, 41, 138–144, doi:10.1038/s41401-019-0228-6.

 doi:10.20944/preprints202505.2096.v1

31. Dallakyan, S.; Olson, A.J. Small-Molecule Library Screening by Docking with PyRx. *Chem Biol: Methods Mol. Biol.* **2015**, 1263, 243-250, doi: 10.1007/978-1-4939-2269-7_19.
32. Umi-Baroroh, S.; Biotek, M.; Muscifa, Z. S.; Destiarani, W.; Rohmatullah, F. G.; Yusuf, M. Molecular interaction analysis and visualization of protein-ligand docking using Biovia Discovery Studio Visualizer. *I.J.C.B.* **2023**, 2, 1, 22–30. https://doi.org/10.24198/ijcb.v2i1.46322
33. Kim, S.; Chen, J.; Cheng, T.; Gindulyte, A.; He, J.; He, S.; Li, Q.; Shoemaker, B.A.; Thiessen, P.A.; Yu, B.; et al. PubChem 2025 Update. *Nucleic Acids Res.* **2025**, 53, 1516–1525, doi:10.1093/nar/gkae1059.
34. O'Boyle, N.M.; Banck, M.; James, C.A.; Morley, C.; Vandermeersch, T.; Hutchison, G.R. Open Babel: An Open Chemical Toolbox. *J. Cheminform.* **2011**, *3*, 1–14, doi:10.1186/1758-2946-3-33/FIGURES/1.
35. Jo, S.; Kim, T.; Iyer, V.G.; Im, W. CHARMM-GUI: A Web-Based Graphical User Interface for CHARMM. *J. Comput. Chem.* **2008**, 29, 1859–1865, doi:10.1002/jcc.20945.
36. Piña-Torres, I.H.; Dávila-Berumen, F.; González-Hernández, G.A.; Torres-Guzmán, J.C.; Padilla-Guerrero, I.E. Hyphal Growth and Conidia Germination Are Induced by Phytohormones in the Root Colonizing and Plant Growth Promoting Fungus *Metarhizium Guizhouense*. *J. Fungi* **2023**, *9*, 1-13, doi:10.3390/jof9090945.
37. Estrada-Mata, E.; Navarro-Arias, M.J.; Pérez-García, L.A.; Mellado-Mojica, E.; López, M.G.; Csonka, K.; Gacser, A.; Mora-Montes, H.M. Members of the *Candida parapsilosis* Complex and *Candida albicans* Are Differentially Recognized by Human Peripheral Blood Mononuclear Cells. *Front. Microbiol.* **2016**, 6, 1–11, doi:10.3389/fmicb.2015.01527.
38. Mora-Montes, H.M.; Bates, S.; Netea, M.G.; Díaz-Jiménez, D.F.; López-Romero, E.; Zinker, S.; Ponce-Noyola, P.; Kullberg, B.J.; Brown, A.J.P.; Odds, F.C.; et al. Endoplasmic Reticulum α-Glycosidases of *Candida albicans* Are Required for N Glycosylation, Cell Wall Integrity, and Normal Host-Fungus Interaction. *Eukaryot. Cell* **2007**, 6, 2184–2193, doi:10.1128/EC.00350-07.
39. Tamez-Castrellón, A.K.; van der Beek, S.L.; López-Ramírez, L.A.; Martínez-Duncker, I.; Lozoya-Pérez, N.E.; van Sorge, N.M.; Mora-Montes, H.M. Disruption of Protein Rhamnosylation Affects the *Sporothrix Schenckii*-Host Interaction. *Cell Surf.* **2021**, *7*, 100058, doi:10.1016/j.tcsw.2021.100058.
40. Coutsias, E.A.; Wester, M.J. RMSD and Symmetry. *J Comput. Chem.* **2019**, 40, 1496–1508, doi:10.1002/jcc.25802.
41. Carugo, O. Statistical Validation of the Root-Mean-Square-Distance, a Measure of Protein Structural Proximity. *PEDS* **2007**, 20, 33–37, doi:10.1093/protein/gzl051.
42. Felsenstein, J.; Churchill, G.A. A Hidden Markov Model Approach to Variation Among Sites in Rate of Evolution. *Mol. Biol. Evol.* **1996**, 13, 93–104.
43. Abdel-Azeem, A.M.; Abdel-Azeem, M.A.; Abdul-Hadi, S.Y.; Darwish, A.G. *Aspergillus*: Biodiversity, Ecological Significances, and Industrial Applications. *Fungal Biol.* **2019**, 121–179.
44. Ashiq, S. Natural Occurrence of Mycotoxins in Food and Feed: Pakistan Perspective. *Compr. Rev. Food Sci.* **2015**, 14, 159–175, doi:10.1111/1541-4337.12122.
45. Adeyeye, S.A.O. Fungal Mycotoxins in Foods: A Review. *Cogent. Food Agric.* **2016**, 2, 1-11, doi: 10.1080/23311932.2016.1213127
46. Moretti, A.; Susca, A. *Penicillium* Species and Their Associated Mycotoxins.; *H. Press: New York* **2017**,182, 167-177.
47. Gurikar, C.; Shivaprasad, D.P.; Sabillón, L.; Nanje Gowda, N.A.; Siliveru, K. Impact of Mycotoxins and Their Metabolites Associated with Food Grains. *Grain and Oil Sci. Tech.* **2023**, 6, 1–9.
48. Abdel-Azeem, A.M.; Abdel-Azeem, M.A.; Darwish, A.G.; Nafady, N.A.; Ibrahim, N.A. *Fusarium*: Biodiversity, Ecological Significances, and Industrial Applications. *Fungal Biol.* **2019**, 201–261.
49. Awuchi, C.G.; Ondari, E.N.; Ogbonna, C.U.; Upadhyay, A.K.; Baran, K.; Okpala, C.O.R.; Korzeniowska, M.; Guiné, R.P.F. Mycotoxins Affecting Animals, Foods, Humans and Plants: Types, Occurrence, Toxicities, Action Mechanisms, Prevention and Detoxification Strategies-a Revisit. *Foods* **2021**, 10.
50. Qiu, J.; Dong, F.; Yu, M.; Xu, J.; Shi, J. Effect of Preceding Crop on Fusarium Species and Mycotoxin Contamination of Wheat Grains. *J. Sci. Food Agric.* **2016**, 96, 4536–4541, doi:10.1002/jsfa.7670.
51. Chiotta, M.L.; Fumero, M.V.; Cendoya, E.; Palazzini, J.M.; Alaniz-Zanon, M.S.; Ramirez, M.L.; Chulze, S.N. Toxigenic Fungal Species and Natural Occurrence of Mycotoxins in Crops Harvested in Argentina. *Rev. Argent. Microbiol.* **2020**, 52, 339–347, doi:10.1016/j.ram.2020.06.002.

 doi:10.20944/preprints202505.2096.v1

52. Candadai S. Ramadoss; John Uhlig; Don M. Carbon; Larry G. Butler; Ralph L. Nicholson Composition of the Mucilaginous Spore Matrix of *Colletotrichum*, a Pathogen of Corn, Sorghum, and Other Grasses. *ACS* **1985**, 33.
53. Poveda, J. *Trichoderma* as Biocontrol Agent against Pests: New Uses for a Mycoparasite. *Biological Control* **2021**, 159.
54. Guzmán-Guzmán, P.; Porras-Troncoso, M.D.; Olmedo-Monfil, V.; Herrera-Estrella, A. *Trichoderma* Species: Versatile Plant Symbionts. *Phytopathol.* **2019**, 109, 6–16.
55. Sheshegova, T.K.; Shchekleina, L.M. Control of Ergot (*Claviceps purpurea* (Fr) Tul.) with New Pesticides. *Russ. Agric. Sci.* **2020**, 46, 472–475, doi:10.3103/s1068367420050183.
56. Chen, W.; Yu, M.; Chen, S.; Gong, T.; Xie, L.; Liu, J.; Bian, C.; Huang, G.; Zheng, C. Structures and Biological Activities of Secondary Metabolites from *Xylaria* Spp. *J. Fungi* **2024**, 10.
57. Koyani, R. Xylariaceae: Overview and Addition to Fungal Diversity of Gujarat State. *Stud. Fungi* **2016**, 1, 69–79, doi:10.5943/sif/1/1/6.
58. Prillinger, H.; Lopandic, K. Yeast-Types of the Basidiomycota Using Cell Wall Sugars and Ribosomal DNA Sequences. *STAPFIA* **2015**, 103, 3–18.
59. Rytioja, J.; Hildén, K.; Di Falco, M.; Zhou, M.; Aguilar-Pontes, M.V.; Sietiö, O.M.; Tsang, A.; de Vries, R.P.; Mäkelä, M.R. The Molecular Response of the White-Rot Fungus *Dichomitus squalens* to Wood and Non-Woody Biomass as Examined by Transcriptome and Exoproteome Analyses. *Environ. Microbiol.* **2017**, 19, 1237–1250, doi:10.1111/1462-2920.13652.
60. Rytioja, J.; Hildén, K.; Yuzon, J.; Hatakka, A.; de Vries, R.P.; Mäkelä, M.R. Plant-Polysaccharide-Degrading Enzymes from Basidiomycetes. *Microbio. Mol. Bio. Rev.* **2014**, 78, 614–649, doi:10.1128/mmbr.00035-14.
61. Liers, C.; Arnstadt, T.; Ullrich, R.; Hofrichter, M. Patterns of Lignin Degradation and Oxidative Enzyme Secretion by Different Wood- and Litter-Colonizing Basidiomycetes and Ascomycetes Grown on Beech-Wood. *FEMS Microbiol. Ecol.* **2011**, 78, 91–102, doi:10.1111/j.1574-6941.2011.01144.x.
62. López, S.C.; Peng, M.; Issak, T.Y.; Daly, P.; de Vries, R.P.; Mäkelä, M.R. Induction of Genes Encoding Plant Cell Wall-Degrading Carbohydrate-Active Enzymes by Lignocellulose-Derived Monosaccharides and Cellobiose in the White-Rot Fungus *Dichomitus* squalens. *Appl. Environ. Microbiol.* **2018**, 84, doi:10.1128/AEM.00403-18.
63. Santhanam, P.; Boshoven, J.C.; Salas, O.; Bowler, K.; Islam, M.T.; Saber, M.K.; van den Berg, G.C.M.; Bar-Peled, M.; Thomma, B.P.H.J. Rhamnose Synthase Activity Is Required for Pathogenicity of the Vascular Wilt Fungus *Verticillium dahliae*. *Mol. Plant Pathol.* **2017**, 18, 347–362, doi:10.1111/mpp.12401.
64. Xie, X.; Lipke, P.N. On the Evolution of Fungal and Yeast Cell Walls. *Yeast* **2010**, 27, 479–488.
65. Klaubauf, S.; Tharreau, D.; Fournier, E.; Groenewald, J.Z.; Crous, P.W.; de Vries, R.P.; Lebrun, M.H. Resolving the Polyphyletic Nature of *Pyricularia* (Pyriculariaceae). *Stud. Mycol.* **2014**, 79, 85–120, doi:10.1016/j.simyco.2014.09.004.
66. Luo, J.; Zhang, N. *Magnaporthiopsis*, a New Genus in Magnaporthaceae (Ascomycota). *Mycol.* **2013**, 105, 1019–1029, doi:10.3852/12-359.
67. Martyn, R.D.; Miller, M.E. *Monosporascus* Root Rot and Vine Decline. *APS* **1996**, 80, 716–725.
68. Hugouvieux, V.; Centis, S.; Lafitte, C.; Esquerre-Tugaye, M.-T. Induction By-L-Arabinose and-L-Rhamnose of Endopolygalacturonase Gene Expression in *Colletotrichum lindemuthianum*. *Appl. Environ. Microbiol.* **1997**, 63.
69. Ahmed, A.O.A.; van Leeuwen, W.; Ahmed, F.; van de Sande, W.; Verbrugh, H.; van Belkum, A. Madurella Caused by *Madurella Mycetomatis*: A Infectious Burden. *Lancet. Infect. Dis.* **2004**, 4, 566–574.
70. Rolshausen, P.E.; Baumgartner, K.; Travadon, R.; Fujiyoshi, P.; Pouzoulet, J.; Wilcox, W.F. Identification of *Eutypa* Spp. Causing Eutypa Dieback of Grapevine in Eastern North America. *Plant Dis.* **2013**, 98, 483–491, doi:10.1094/PDIS-08-13-0883-RE.
71. Gavrilova, O.P.; Orina, A.S.; Kessenikh, E.D.; Gustyleva, L.K.; Savelieva, E.I.; Gogina, N.N.; Gagkaeva, T.Y. Diversity of Physiological and Biochemical Characters of *Microdochium* Fungi. *Chem. Biodivers.* **2020**, 17, doi:10.1002/cbdv.202000294.
72. Petrović, E.; Godena, S.; Ćosić, J.; Vrandečić, K. Identification and Pathogenicity of *Biscogniauxia* and *Sordaria* Species Isolated from Olive Trees. *Horticul.* **2024**, 10, doi:10.3390/horticulturae10030243.

 doi:10.20944/preprints202505.2096.v1

73. Lopez, D.C.; Zhu-Salzman, K.; Ek-Ramos, M.J.; Sword, G.A. The Entomopathogenic Fungal Endophytes *Purpureocillium lilacinum* (Formerly *Paecilomyces lilacinus*) and *Beauveria bassiana* Negatively Affect Cotton Aphid Reproduction under Both Greenhouse and Field Conditions. *PLoS One* **2014**, 9, doi:10.1371/journal.pone.0103891.
74. Wiggins, C.A.R.; Munro, S. Activity of the Yeast MNN1-1,3-Mannosyltransferase Requires a Motif Conserved in Many Other Families of Glycosyltransferases. *Proc. Natl. Acad. Sci. U.S.A.* **1995**, 14, 7945-7950
75. Schuman, B.; Alfaro, J.A.; Evans, S. V. Glycosyltransferase Structure and Function. In Bioactive Conformation I. *Sprin. Berl. Heidel.* **2006**, 217–257.
76. Lairson, L.L.; Henrissat, B.; Davies, G.J.; Withers, S.G. Glycosyl Transferases: Structures, Functions, and Mechanisms. *Annu. Rev. Biochem.* **2008**, 77, 521–555.
77. Eck, R. V; Dayhoff, M.O. Evolution of the Structure of Ferredoxin Based on Living Relics of Primitive Amino Acid. *Science* **1966**, 15, 152.
78. Zong, G.; Fei, S.; Liu, X.; Li, J.; Gao, Y.; Yang, X.; Wang, X.; Shen, Y. Crystal Structures of Rhamnosyltransferase UGT89C1 from *Arabidopsis thaliana* Reveal the Molecular Basis of Sugar Donor Specificity for UDP-β-l-Rhamnose and Rhamnosylation Mechanism. *Plant J.* **2019**, 99, 257–269, doi:10.1111/tpj.14321.
79. Brazier-Hicks, M.; Offen, W.A.; Gershater, M.C.; Revett, T.J.; Lim, E.-K.; Bowles, D.J.; Davies, G.J.; Edwards, R.; Designed, G.J.D.; Performed, G.J.D. Characterization and Engineering of the Bifunctional N-and O-Glucosyltransferase Involved in Xenobiotic Metabolism in Plants. *Proceed. Nat.l Acad. Sci.* **2007**, 104, 20238–20243.
80. Ren, C.; Guo, Y.; Xie, L.; Zhao, Z.; Xing, M.; Cao, Y.; Liu, Y.; Lin, J.; Grierson, D.; Zhang, B.; et al. Identification of UDP-Rhamnosyltransferases and UDP-Galactosyltransferase Involved in Flavonol Glycosylation in *Morella rubra*. *Hortic. Res.* **2022**, 9, doi:10.1093/hr/uhac138.
81. Ruiz-Herrera, J.; Ortiz-Castellanos, L. Cell Wall Glucans of Fungi. A Review. *Cell Surf.* **2019**, 5.
82. Kadry, A.A.; El-Ganiny, A.M.; Mosbah, R.A.; Kaminskyj, S.G.W. Deletion of *Aspergillus nidulans* GDP-Mannose Transporters Affects Hyphal Morphometry, Cell Wall Architecture, Spore Surface Character, Cell Adhesion, and Biofilm Formation. *Med. Mycol.* **2018**, 56, 621–630, doi:10.1093/mmy/myx082.
83. Rizza, V.; Kornfeld, J.M. Components of Conidial and Hyphal Walls of *Penicillium chrysogenum*. *Microbiol. Soc.* **1969**, 58.
84. Pettolino, F.; Sasaki, I.; Turbic, A.; Wilson, S.M.; Bacic, A.; Hrmova, M.; Fincher, G.B. Hyphal Cell Walls from the Plant Pathogen *Rhynchosporium secalis* Contain (1,3/1,6)-β-D-Glucans, Galacto- and Rhamnomannans, (1,3;1,4)-β-D- Glucans and Chitin. *FEBS J.* **2009**, 276, 3698–3709, doi:10.1111/j.1742-4658.2009.07086.x.
85. Martinez, V.; Ingwers, M.; Smith, J.; Glushka, J.; Yang, T.; Bar-Peled, M. Biosynthesis of UDP-4-Keto-6-Deoxyglucose and UDP-Rhamnose in Pathogenic Fungi *Magnaporthe grisea* and *Botryotinia fuckeliana*. *J. Biol. Chem.* **2012**, 287, 879–892, doi:10.1074/jbc.M111.287367.
86. Do Carmo-Sousa, L.; Barroso-Lopes, C. A Comparative Study of the Extracellular and Cell-Wall Polysaccharides of Some *Candida* Species. *Antonie van Leewenhoek* **1970**, 36, 209–216.